TIE2 activation by antibody-clustered endogenous angiopoietin-2 prevents capillary loss and fibrosis in experimental kidney disease

Authors: Riikka Pietilä[1], Amanda Marks Hultström[1], Liqun He[1], Sami Nanavazadeh[1], Susan E Quaggin[2], Christer Betsholtz[1,3], and Marie Jeansson[1,3] *

Affiliations:

[1]Department of Immunology, Genetics and Pathology, Uppsala University; Uppsala, Sweden.

[2]Feinberg Cardiovascular Research Institute and Division of Nephrology and Hypertension, Northwestern University; Chicago, IL, USA.

[3]Department of Medicine Huddinge, Karolinska Institutet; Huddinge, Sweden.

*Corresponding author. Marie Jeansson, Department of Medicine Huddinge, Blickagangen 16, 141 62 Huddinge, Sweden. Phone +45 791679182. Email: marie.jeansson@ki.se

Conflict-of-interest statement: MJ is the inventor on a filed patent (PCT/EP2025/056090) "ANGPT2-targeting antibodies for use in the treatment of kidney disease(s), disorder(s) or injury associated with kidney fibrosis", owns stock in, and is a director of Sang Biotech AB. CB owns stock in Sang Biotech AB. SEQ holds patents related to therapeutic targeting of the ANGPT-TEK pathway in ocular hypertension, glaucoma, and acute kidney injury and receives research support, owns stock in, and is a director of Mannin Research. The other authors declare no conflicts of interest.

ABSTRACT

The role of endothelial dysfunction in tubulointerstitial fibrosis associated with chronic kidney disease (CKD) is not well understood. In this study, we demonstrate that the activation of the endothelial tyrosine kinase TIE2 alleviates renal pathology in experimental CKD in mice. TIE2 activation was achieved using a human angiopoietin-2 (ANGPT2)-binding and TIE2-activating antibody (ABTAA), or through adult-induced endothelial-specific knockout of the vascular endothelial protein tyrosine phosphatase gene (*Veptp*). Both methods markedly protected CKD mice from endothelial dysfunction, peritubular capillary loss, tubular epithelial injury, and tubulointerstitial fibrosis. Conversely, silencing TIE2 through adult-induced endothelial-specific knockout of the *Tie2* gene exacerbated CKD pathology. Additionally, we found that endothelial dysfunction promotes renal fibrosis not through endothelial-to-mesenchymal transition as previously expected, but by inducing the expression of pro-fibrotic PDGFB in tubular epithelial cells, a process that is inhibited by TIE2 activation. Our findings suggest that TIE2 activation via ABTAA warrants investigation as a therapy in human CKD, where there is a substantial unmet medical need.

INTRODUCTION

Chronic kidney disease (CKD) affects approximately13% of the global population and is a leading cause of death due to cardiovascular disease (1-3). It is projected that CKD will rank as the 5th leading cause of death by 2040 (4). While various conditions, such and diabetes and hypertension, can lead to CKD, the common pathogenic pathway typically involves endothelial dysfunction, capillary rarefaction, tubular atrophy, and tubulointerstitial fibrosis, as observed in both animal models and patients (5-18). With no cure available and only a limited number of therapies to slow its progression, there is an urgent need to identify and develop new and effective treatments against CKD. Despite extensive research into the mechanism underlying renal fibrosis, the role and dysregulation of the vasculature, as well as its contributions to tubular injury and fibrosis, remain inadequately understood.

TIE2, also known as TEK, is a tyrosine kinase receptor primarily expressed by endothelial cells. The phosphorylation of TIE2 and thereby triggered downstream signaling pathways promote vascular quiescence and reduce vascular permeability, inflammation, and endothelial apoptosis (19-21). The activity of TIE2 is regulated by angiopoietin (ANGPT) ligands, specifically ANGPT1 and ANGPT2, as well as the vascular endothelial tyrosine phosphatase VEPTP. Research has shown that ANGPT1, the primary agonist for TIE2, is decreased in both CKD patients and experimental models (5, 22-26). Conditional deletion of *Angpt1* has resulted in more severe kidney injury in cases of diabetes and obstruction-induced CKD (5, 24). Conversely, circulating levels of ANGPT2, which acts as a context-dependent antagonist of TIE2, increase in CKD patients and correlate with adverse cardiovascular and renal outcomes (27-31). Inhibition of ANGPT2 has recently been shown to reduce kidney injury in experimental CKD (27).

VEPTP is a phosphatase that decreases tyrosine phosphorylation of several proteins, including TIE2 (32, 33). VEPTP is upregulated in experimental models of diabetes and ischemia-reperfusion injury, and conditional knockout of *Veptp* has been found to increase the activity of TIE2 and reduce kidney injury (34, 35). ANGPT1, as well as ANGPT1-mimetics and transgenic expression of *Angpt1*, have demonstrated beneficial effects in various preclinical models of kidney injury (23, 25, 26, 35-38). However, limitations related to production, storage, half-life, applicability, and efficacy of these compounds have hindered their clinical use in CKD. ABTAA is an angiopoietin-2 binding and TIE2 activating antibody (39) that clusters endogenous ANGPT2 into a complex, enabling TIE2 activation and vascular normalization. ABTAA has shown protective effects in sepsis-induced kidney injury (39), causes tumor vessel normalization (40), and promotes choriocapillary regeneration in macular degeneration (41). Notably, ABTAA offered greater protection in sepsis compared to ANGPT2 inhibition alone, underscoring its dual functional advantage (39).

While it is widely recognized that both endothelial dysfunction and tubulointerstitial fibrosis occur in CKD, the relationship between the two remains unclear. Tubulointerstitial fibrosis develops when perivascular mesenchymal cells, normally responsible for structurally and functionally supporting capillaries (42), become activated, proliferate, migrate, and deposit extracellular matrix (ECM) (43-47). Platelet-derived growth factor-B (PDGFB) acts as a mitogen for perivascular mesenchymal cells expressing the PDGF receptor-β (PDGFRB), and is necessary for the proper recruitment and maintenance of pericytes around capillaries (42, 48). PDGFB/RB signaling has been associated with fibrosis; for example, constitutive activation of PDGFRB in mesenchymal cells has been shown to result in spontaneous renal fibrosis (49), while inhibition of PDGFB or PDGFRB has reduced fibrosis in experimental CKD models (50-56). A highly debated mechanism

for the development of renal fibrosis is the notion that activated mesenchymal cells originate from endothelial-to-mesenchymal transition (EndoMT) (57).

In this study, we investigated how endothelial dysfunction and inactivation of TIE2 signaling in CKD affect tubular injury and PDGFB-driven tubulointerstitial fibrosis. Additionally, we explored whether treatment with an ANGPT2-binding and TIE2-activating antibody, ABTAA, could serve as an effective therapy for renal injury associated with experimental CKD.

RESULTS

Pharmacological or genetic activation of TIE2 improves renal perfusion and prevents capillary rarefaction following experimental CKD

We investigated the role of TIE2 signaling through gain- and loss-of-function experiments utilizing the unilateral ureter obstruction (UUO) model, a widely used progressive model of CKD (5). UUO injury is characterized by capillary rarefaction and tubulointerstitial fibrosis (5, 16, 58) in the obstructed kidney, while the contralateral kidney serves as a control (Figure 1A). ABTAA treatment or conditional endothelial knockout of *Veptp* (*Veptp*^{iECKO}) was employed to induce TIE2 activation (Figure 1A-C). In contrast, conditional endothelial knockout of *Tie2* (*Tie2*^{iECKO}) was used as a model of TIE2-incompetent signaling. We investigated the causal effect of PDGFB on tubulointerstitial fibrosis using a conditional global knockout of *Pdgfb* (*Pdgfb*^{iKO}) (Figure 1C).

ABTAA requires ANGPT2 to activate TIE2 (39), and increased levels of ANGPT2 was confirmed in UUO kidneys (Supplemental Figure S1A, B). However, circulating ANGPT2 levels remained unchanged, indicating that the injury, and resulting ANGPT2 expression, are localized to UUO kidneys (Supplemental Figure S1C). Both ABTAA treated and *Veptp*^{iECKO} mice exhibited increased TIE2 phosphorylation in the UUO kidneys (Figure 1D, E; Supplemental Figure S2). Importantly, ABTAA did not induce systemic TIE2 activation, as demonstrated by the unchanged TIE2 phosporylation levels in lung tissue (Supplemental Figure S1D), contrasting the broad effects observed in *Veptp*^{iECKO} (34). UUO resulted in increased VEPTP levels and decreased TIE2 expression (Figure 1F, G). Both *Veptp*^{iECKO} and *Tie2*^{iECKO} showed significant reductions in their respective protein expressions (Figure 1F, G; Supplemental Figure S3).

Renal perfusion was assessed using contrast-enhanced ultrasound imaging. The UUO-induced reduction in renal perfusion was significantly prevented in ABTAA-treated and *Veptp*^{iECKO} mice

compared to IgG-treated and wildtype (WT) controls. The *Pdgfb*^{iKO} did not affect renal perfusion. In contrast, the *Tie2*^{iECKO} mice exhibited significantly lower UUO-induced renal perfusion compared to WT mice (Figure 1H). The disadvantage in *Tie2*^{iECKO} was apparent after just 1 day of UUO, where microangiopathy indicated a significant reduction in perfused capillaries in *Tie2*^{iECKO} mice but not in WT mice (Supplemental Figure S4A, B).

Peritubular capillary (PTC) density in the renal cortex was evaluated using immunostaining for the endothelial markers endomucin and podocalyxin (59). UUO-induced PTC rarefaction was significant in the kidneys subjected to 3-day UUO compared to the contralateral kidneys. Both ABTAA treatment and *Veptp*^{iECKO} significantly prevented the loss of PTCs, while *Tie2*^{iECKO} mice experienced exacerbated capillary rarefaction. The *Pdgfb*^{iKO} did not influence UUO-induced capillary rarefaction (Figure 1I-K).

Pharmacological or genetic TIE2 activation prevents UUO-induced endothelial injury

Fenestrations in PTCs are essential structures for reabsorption of water and solutes from the tubular system. These fenestrations are known to be reduced in CKD and can serve as indicators of capillary dysfunction (16). In the contralateral kidneys, all groups of animals displayed healthy, continuous fenestrations of PTCs (Figure 2A, B). The UUO-induced reduction in fenestrations was significantly prevented in ABTAA-treated and *Veptp*^{iECKO} mice compared to IgG-treated and WT controls. In contrast, the UUO kidneys in *Tie2*^{iECKO} mice exhibited a significantly greater loss of fenestrations compared to UUO kidneys in WT mice (Figure 2A, B).

UUO injury had no impact on glomerular vessels and podocytes in WT and *Tie2*^{iECKO} mice (Supplemental Figure S5), also seen previously (60). Despite the evident capillary rarefaction observed in kidneys subjected to 3 days of UUO, endothelial cells remained present in the tissue

following the injury. Endothelial nuclei labeled with lineage tracer *Cdh5*-TdTomato remained consistent in kidneys after 3 days of UUO (Figure 2C), indicating that the reduced capillary density does not merely reflect endothelial cell death. However, 10 day UUO kidneys showed a significant loss of endothelial nuclei in the cortex, with a further reduction in *Tie2*^{iECKO} mice (Figure 2C). This reduction was not a result of altered cell proliferation, as both Ki67 staining and EdU incorporation demonstrated similar responses in WT and *Tie2*^{iECKO} mice (Supplemental Figure S6A-D). Furthermore, the *Cdh5*-TdTomato lineage reporter overlapped with endomucin staining in PTCs of both WT and *Tie2*^{iECKO} mice up to 10 days post-UUO (Figure 2D).

Pharmacological or genetic TIE2 activation prevents UUO-induced tubulointerstitial fibrosis

The activation of perivascular mesenchymal cells into myofibroblasts is characterized by the expression of alpha-smooth muscle actin (aSMA) and vimentin, as well as the production of ECM components, including type I collagen and fibronectin (61, 62). Fibrosis in the renal cortex was quantified by staining for aSMA and vimentin. UUO-induced fibrosis was significantly reduced in ABTAA-treated and *Veptp*^{iECKO} mice compared to controls (Figure 3A-C). A similar trend (reduction) was seen was noted for *Col1a1* and *Pdgfrb* in ABTAA-treated and *Pdgfb*^{iKO} mice, respectively (Figure 3D, E). Additionally, *Pdgfb*^{iKO} mice exhibited significantly reduced fibrosis (Figure 3A-C), supporting the role of PDGFB as a major mesenchymal cell activator following UUO. In contrast, *Tie2*^{iECKO} mice displayed markedly more fibrosis in their 3-day UUO kidneys, along with increased expression of *Col1a1*, *Tagln*, and *Fn1* (Figure 3F).

Collectively, our data demonstrates that the protective role of ABTAA on vascular integrity also effectively reduces tubulointerstitial fibrosis, the final pathological process in CKD.

UUO-induced tubulointerstitial fibrosis is not the result of EndoMT

EndoMT has been suggested to contribute to fibrosis in CKD models including UUO (63). To investigate this, we introduced a fibroblast-specific nuclear *Pdgfra*-H2BGFP (64) allele into the *Tie2*^{iECKO} line, resulting in WT and *Tie2*^{iECKO} mice that had both an endothelial-specific linage reporter (*Cdh5*-TdTomato) and a mesenchymal/myofibroblast reporter (nuclear-located GFP) (Figure 4A). *Tie2*^{iECKO} mice were included in the experiment because they exhibit worse endothelial injury after UUO than WT mice, thus representing a model with more unstable endothelial cells. RNA-ISH for *Pdgfra* and *Pdgfrb* revealed that mesenchymal cells responding to UUO are positive for both markers, suggesting that fibrosis is primarily driven by dual-expressing *Pdgfra*/*Pdgfrb* cells (Supplemental Figure 6F).

As expected, the number of *Pdgfra*-H2BGFP+ cells increased significantly in the renal cortex of kidneys subjected to 3 and 10 days of UUO. However, no differences were observed between WT and *Tie2*^{iECKO} mice in the number of *Pdgfra*-H2BGFP+ cells after 3 or 10 day UUO (Figure 4B, C). These findings suggest that the increased tubulointerstitial fibrosis seen during disease progression and in *Tie2*^{iECKO} mice reflects a change in the activation state of mesenchymal cells rather than a difference in their quantity. Importantly, no *Cdh5*-TdTomato+/*Pdgfra*-H2BGFP+ cells were identified in either group, providing no evidence of UUO-induced EndoMT in WT or *Tie2*^{iECKO} mice (Figure 4B, D). Additionally, tubular epithelial cells were also negative for *Pdgfra*-H2BGFP (Figure 4E).

Thus, our data fail to support endothelial- or epithelial-to-mesenchymal transition as mechanisms for tubulointerstitial fibrosis in the UUO model, indicating that deficient TIE2 signaling does not promote EndoMT in this context.

Pharmacological or genetic TIE2 activation prevents UUO-induced tubular injury and PDGFB expression

The renal tubular system is densely packed with mitochondria and relies on oxidative phosphorylation, making it vulnerable to ischemic injury (65). We aimed to analyze whether TIE2 activation in the vasculature could protect the tubular system in our CKD model. UUO-induced tubular vacuoles were assessed as an indicator of tubular injury (for details, see Methods) (Figure 5A). Cortical tubular segments exhibiting UUO-induced pathological vacuoles were significantly reduced in ABTAA-treated and *Veptp*^{iECKO} mice compared to IgG-treated and WT controls (Figure 5B). In contrast, *Tie2*^{iECKO} mice showed substantially greater tubular injury compared to WT mice (Figure 5B).

PDGFB is a known mitogen for perivascular mesenchymal cells and upregulated in kidney diseases (66). While TIE2 has been shown to regulate *Pdgfb* in endothelial cells (67, 68), our RNA *in situ* hybridization (RNA-ISH) analysis revealed that *Pdgfb* expression was significantly upregulated in tubular segments following UUO, with no effect on isolated endothelial cells (Figure 5C, Supplemental Figure S6E). This finding, along with recent single-cell RNA sequencing data in experimental CKD (47, 69), supports the idea of using *Pdgfb* as a marker for tubular injury.

To further investigate the early regulation of injury markers, we performed gene expression analysis at 6, 12, and 24 hours after UUO. We observed a notable and sustained increase in kidney injury molecule 1 (*Kim1/Havcr1*) and *Pdgfb*, beginning at 6 hours post-UUO, indicating early tubular injury (Figure 5D). At these early timepoints, mesenchymal activation had not yet occurred, as indicated by the stable *Pdgfrb* expression throughout the analysis. UUO also led to

reduced expression of both *Tie2*/*Tek* and *Angpt1* (Figure 5D). *Angpt1* expression was also suppressed 3 and 10 days after UUO (Figure 5D), which we have previously shown (5). RNA-ISH demonstrated that *Angpt1* was expressed in both mesenchymal cells and tubular epithelial cells, with UUO-induced reductions primarily affecting tubular cells (Figure 5F).

Importantly, UUO-induced expression of *Pdgfb*/PDGFB was significantly prevented in ABTAA-treated and *Veptp*^{iECKO} mice (Figure 5G, H), supporting the notion of vascular-mediated protection of the tubular system. As expected, *Pdgfb*^{iKO} mice exhibited reduced *Pdgfb* expression in both UUO and contralateral (unobstructed) kidneys (Figure 5I). Our data support a sequence of events whereby vascular integrity regulates tubular injury and PDGFB expression, which in turn influences the degree of tubulointerstitial fibrosis. Notably, patients with CKD or renal dysfunction display changes in corresponding genes, such as a loss of the endothelial marker CDH5, an increase in *ANGPT2* and *PDGFB*, and a reduction in *ANGPT1* (Figure 5J).

Post-injury treatment with ABTAA slows progression of fibrosis. To further investigate the therapeutic potential of ABTAA treatment, we implemented a more clinically relevant treatment regimen. Specifically, we initiated ABTAA treatment 3 days after UUO injury and assessed the kidneys at day 10 (Figure 6A). In this context, UUO-induced capillary density in the ABTAA-treated mice was similar to that observed in the IgG treated mice (Figure 6B-D). However, post-injury ABTAA treatment significantly reduced UUO-induced tubulointerstitial fibrosis, as indicated by aSMA and vimentin staining, while *Tie2*^{iECKO} mice exhibited a significant increase in fibrosis (Figure 6E, F). Additionally, tubular injury, as reflected by PDGFB expression, was notably prevented in ABTAA-treated mice, suggesting improved vascular function, although this may not be due to preserved capillary density (Figure 6G).

Pharmacological or genetic TIE2 activation, or inhibition of PDGFB signaling, protect the kidney transcriptome following UUO injury

Bulk RNA-seq of whole kidneys was used to investigate transcriptional changes in ABTAA-treated, *Veptp*^{iECKO}, and *Pdgfb*^{iKO} mice 3 days post-UUO. We visualized genes associated with ECM modification, tubular injury, endothelial function, and inflammation in heatmaps across our experimental groups (Figure 7A; Supplemental File 1). As expected, UUO-induced ECM modification genes, including *Acta2, Col1a1, Col1a2, Col3a1, Col4a1, Pdgfrb, Fn1, Tagln, Dcn, Cnn2, Tnc, Mmp2, Timp2, and Adamts1*, along with tubular injury markers such as *Havcr1, Lcn2, Clu, Piezo1, Krt8, Ets2, Rela,* and *Pdgfb*, were significantly upregulated compared to the contralateral kidneys in their respective groups. Both ABTAA treatment and *Veptp*^{iECKO} exhibited a generally reduced response, though most did not reach statistical significance (Figure 7A; Supplemental File 2). Notably, *Pdgfb*^{iKO} demonstrated significant protection against most ECM modification- and tubular injury genes. Only a few of the endothelial genes (*Pecam1, Emcn, Cdh5, Tek, Tie1, Ptprb, Angpt2, Plvap, Kdr, Flt1*) were significantly regulated (Figure 7A), despite the pronounced capillary rarefaction and loss of fenestrations documented in experimental data (Figure 1, 2). The Discussion section addresses potential reasons for these observations. UUO-induced endothelial activation markers (*Klf4, Icam1, Vcam1*) were present in several injured kidneys but were partly blunted in ABTAA-treated, *Veptp*^{iECKO}, and *Pdgfb*^{iKO} mice without reaching statistical significance for most cases (Figure 7A; Supplemental File 2). Overall, the inflammatory response was relatively low (see Discussion), although an increase in UUO-induced macrophage markers (*Adgre1, Cd68, Mrc1, Ccr2*) was observed in *Veptp*^{iECKO} and *Pdgfb*^{iKO} mice, unlike markers for neutrophils (*Cd33*), T-cells (*Cd3e*) nor B-cells (*Ms4a1, Cd19*) (Figure 7A). A

searchable database for all genes is available here https://heomics.shinyapps.io/Jeansson_lab_kidney_UUO/

We subsequently conducted a more in-depth analysis of differentially expressed genes (DEGs) in ABTAA-treated animals compared to controls treated with IgG (Figure 7B, C). In IgG-treated mice, UUO-induced kidney injury resulted in downregulation of 1482 genes and upregulation of 1216 genes compared to contralateral kidneys. In contrast, ABTAA treatment exhibited a blunted response, with 1055 genes downregulated and 984 upregulated DEGs (Figure 7B, C; Supplemental File 2, 3). To elucidate the differences in transcriptional programs, we performed gene ontology (GO) enrichment analysis for unique and common UUO-induced DEGs from both ABTAA and IgG treated groups using Metascape (70). The downregulated unique DEGs in the IgG group and the common DEGs between IgG and ABTAA displayed significant alterations in pathways related to metabolic processes and oxidative phosphorylation, likely reflecting tubular injury due to the high metabolic activity and high mitochondrial density of tubular epithelial cells (71). In comparison, the DEGs specific to ABTAA treatment showed a diminished or absent response in terms of metabolic processes and oxidative phosphorylation (Figure 7B; Supplemental File 4).

In contrast, many of the UUO-induced common upregulated DEGs (from both IgG and ABTAA) were associated with response to wounding, ECM, cell adhesion, and collagen and integrin binding (Figure 7C; Supplemental File 4). These pathways were in many cases also significant in IgG-treated animals. Interestingly, ABTAA treatment appeared to partly blunt these effects (Figure 7C; Supplemental File 4).

DISCUSSION

Our study presents evidence that vascular protection through TIE2 activation via ABTAA is a promising novel therapeutic strategy for CKD. ABTAA's unique ability to bind and cluster ANGPT2 into a potent TIE2 activator helps to prevent endothelial dysfunction, tubular injury, and tubulointerstitial fibrosis in experimental CKD. Findings from genetically modified mice supported this conclusion; TIE2 activation resulting from endothelial *Veptp* knockout provided similar benefit, while endothelial *Tie2* knockout mice exhibited worse kidney damage. Our experiments underscore the critical role of vascular protection in maintaining tubular health, as failure in this process leads to increased pro-fibrotic PDGFB expression and subsequent tubulointerstitial fibrosis.

Previous studies have shown that ABTAA normalizes blood vessels in tumors (40), mitigates sepsis and sepsis-induced injury (39), and promotes choriocapillary regeneration in macular degeneration (41). Notably, ABTAA offered greater protection in sepsis compred to ANGPT2 inhibition alone (39), highlighting its dual beneficial effects: (i) the removal of ANGPT2's antagonistic activity on TIE2, and (ii) the enhanced TIE2 signaling through the conversion of ANGPT2 into a higher-order oligomer that effictively activates TIE2 (39). Our current study illustrates that several modifiers of TIE2 signaling, aside from ANGPT2, are dysregulated in experimental CKD. We observed UUO-induced VEPTP expression in the kidney, consistent with previous reports in models of diabetic nephropathy, ischemia-reperfusion injury, and HIF2α overexpression (34, 35). Additionally, *Angpt1* decreased within 6 hours after UUO, shown previously to be expressed by both tubular epithelial cells and perivascular mesenchymal cells (72-74). Although *Angpt1* expression is highest in mesenchymal cells, their relatively low cell number

compared to the epithelial cells suggests that both sources contribute to biologically relevant levels of ANGPT1 in the kidney. RNA-ISH performed 3 days after UUO in this study indicates reduced *Angpt1* expression primarily in tubular epithelial cells. Recent single-cell RNA sequencing data after ischemia/reperfusion injury and UUO have confirmed the reduction of *Angpt1* transcripts in injured or repairing proximal tubular cells, as well as the loss of *Angpt1* in activated mesenchymal cells (myofibroblasts) (73).

From a therapeutic perspective, ABTAA offers several advantages compared to other TIE2-activating strategies. ABTAA activates TIE2 only in the presence of ANGPT2, as demonstrated by Han *et al* (39). This was also confirmed in the current study; systemic administration of ABTAA selectively restored TIE2 phosphorylation in injured kidneys with elevated ANGPT2 levels, without activating TIE2 in healthy, vascular-rich lung tissue. This supports the injury-targeting mechanism of ABTAA and reduces concern for vascular enlargement and venous malformation, previously demonstrated to result from sustained TIE2 overactivation and *Veptp* deletion (35, 75-77). Importantly, VEPTP is not solely dephosphorylating TIE2, and VEPTP targeting may therefore also affect the phosphorylation of other proteins (33, 78). While ABTAA treatment initiated after UUO injury effectively prevents fibrosis, the PTC density was not preserved. Although the vessels may remain functionally improved with late-onset ABTAA treatment, these findings suggest that once capillary integrity and density are compromised, restoration may be challenging, particularly in the rapidly progressing UUO model. Other studies suggest that capillary injury precedes fibrosis in various preclinical models, including UUO, ischemia/reperfusion, and Alport syndrome (17, 73). This is supported by our current study, where experiments from 6 to 24 hours post-UUO revealed effects on vascular and tubular injury markers

prior to detectable mesenchymal cell activation.

Our results demonstrate that kidney injury leads to increased tubular PDGFB expression in CKD, a finding also identified in recent single-cell RNA-seq studies of experimental CKD (47, 69, 73). Importantly, this study shows that vascular TIE2 activation can attenuate increased PDGFB levels. Additionally, we found that knocking out *Pdgfb* reduces tubulointerstitial fibrosis, confirming the significance of this pathway in mesenchymal cell activation and fibrosis, as previously reported (49-56, 79). However, while PDGFB is known to regulate fibrosis, it is noteworthy that *Pdgfb* knockout does not protect against loss of capillary density. Therefore, targeting PDGFB may not be a viable therapeutic approach, especially given that *Pdgfb* knockout leads to a progressive loss of capillary pericyte coverage (48). The roles of EndoMT and epithelial-to-mesenchymal transition (EMT) in renal fibrosis have been widely debated (63, 80, 81). Given TIE2's importance as an endothelial signaling factor, we investigated whether loss of *Tie2* could promote EndoMT in our experimental CKD model. For this purpose, we utilized a *Cdh5*-TdTomato lineage tracer alongside a *Pdgfra*-H2BGFP reporter to identify putative endothelial cells transitioning toward a mesenchymal phenotype. This approach revealed a UUO-induced increase in mesenchymal cells but provided no evidence of EndoMT or EMT contributing to this process.

Several molecular mechanisms have been proposed to explain the beneficial effects of TIE2 activation in providing vascular protection. TIE2 activation triggers a cascade of downstream signaling events that lead to nuclear exclusion of FOXO1, which in turn increases nitric oxide synthase and local NO production —a pathway previously shown to be renoprotective in CKD models (34, 82, 83). Inflammation and macrophage infiltration are integral to the progression of

renal injury in UUO (84) and CKD in general (85). TIE2-activating compounds, including ABTAA and ANGPT2-inhibitors, are known to exhibit anti-inflammatory effects (27, 39). In our current study, the ethical requirement for administrating UUO mice with an analgesic/anti-inflammatory drug potentially damnpened the inflammatory response, which may explain the minimal injury-induced inflammation observed. Our study confirmed the occurrence of capillary rarefaction, and it showed that PTC perfusion and fenestrations were affected by disease progression, in line with findings from Babickova *et al* (16). The energy demands of tubular epithelial cells, particularly proximal tubular epithelial cells, are high, and these cells rely heavily on the functionality of nearby PTCs for their aerobic metabolism. The UUO-induced downregulation of DEGs linked to metabolic processes and oxidative phosphorylation observed in this study likely reflects injury to tubular epithelial cells, as they represent the majority of cells in the kidney.

While our study was limited to a single experimental model of CKD, the regulation of TIE2 signaling appears to be consistent across various studies and experimental models. ANGPT1, ANGPT1 mimetics, modified ANGPT1, genetic overexpression of *Angpt1*, *Veptp* knockout, and ANGPT2 inhibition have all demonstrated protective effects in preclinical models of kidney injury including UUO, ischemia/reperfusion, and conditions induced by diabetes (including *db/db*, streptozotocin-induced and *Akita* mice), cyclosporin, and sepsis (23, 25-27, 35-38). Our bulk RNA-seq data for individual genes showed trends matching other experimental findings within our study regarding ECM regulation and tubular injury, but statistically significant differences were not reached for most transcripts. Neither capillary rarefaction nor loss of markers of fenestration were observed in our RNA-seq data. While post-transcriptional mechanisms and

protein half-life can contribute to discrepancies between mRNA and protein data, the likely explanation in this case is that the experiment was underpowered (n=4/group). Variability was high in the groups due to treatment effects or gene knockout, compounded by the kidney injury model. It is also possible that the use of whole kidney tissue in RNA-seq did not accurately reflect changes seen in the cortex.

In conclusion, our data demonstrate that CKD progression is regulated by TIE2 signaling and endothelial dysfunction. We further show that ABTAA acts locally in conjunction with increased ANGPT2 levels to protect the renal endothelium, which in turn preserves tubular health, downregulates tubular PDGFB expression, and limit tubulointerstitial fibrosis. These findings provide mechanistic insights into kidney disease progression and offer a strong rational for further testing of ABTAA as a treatment of kidney disease in clinical trials.

MATERIALS AND METHODS

Sex as a biological variable

Our study examined male and female animals, and similar findings are reported for both sexes. Sex as a biological variable was not the subject of the study and some groups have an imbalanced sex distribution, hence, we report the sex in each graph (females: magenta, males: cyan) but do not draw any conclusions about sex differences in the study.

Study design

The major objective of this study was to characterize TIE2 signaling in progression of CKD and to investigate the therapeutic value of TIE2 activation. Mice were subjected to unilateral ureter obstruction (UUO) as an experimental model of CKD. Kidney injury was evaluated up to 10 days after injury. Treatment with ABTAA was used as a pharmacological approach to activate TIE2 and reduce kidney injury after UUO. Similarly, Cre-dependent endothelial specific knockout of *Veptp* was used to genetically increase TIE2 activation. Conditional endothelial knockout of *Tie2* served as a TIE2-incompetent signaling model. The causal effect of PDGFB on tubulointerstitial fibrosis was investigated with conditional global knockout of *Pdgfb*.

Animals

Floxed *Veptp* (34) and *Tie2* (86, 87) mice were crossed with tamoxifen inducible *Cdh5*-Cre^{ERT2} mice (88) to generate endothelial specific knockout of the gene (*Tie2*^{iECKO} and *Veptp*^{iECKO}, respectively). *Tie2* mice were also crossed with a reporter mouse, Ai14-TdTomato (Gt(ROSA)26Sor$^{tm14(CAG-tdTomato)Hze}$, JAX stock 007914) (89), resulting in lineage tag of

endothelial cells. Littermate controls were tamoxifen induced *Tie2* wt/wt; *Cdh5*-Cre^{ERT2} mice for the *Tie2* knockouts and non-induced *Veptp* wt/lox; *Cdh5*-Cre^{ERT2} for *Veptp* knockouts. Floxed *Pdgfb* mice (Pdgfb^{tm2Cbet}) (90) were crossed with tamoxifen inducible *Actb*-Cre^{ERT2} mice (Tg(CAG-cre/Esr1*)5Amc, JAX stock 004682) (91) to generate whole body knockout of *Pdgfb* (*Pdgfb*^{iKO}). Littermate controls were Cre negative *Pdgfb* wt/lox or lox/lox mice. Recombination was induced with 3 doses of tamoxifen (2 mg) in peanut oil by oral gavage at 4 weeks of age (*Tie2*^{iECKO} and *Veptp*^{iECKO}), or 1 week prior to experiments (*Pdgfb*^{iKO}). For some experiments, additional crossings were done to obtain a reporter for myofibroblasts with *Pdgfra*-H2BGFP (Pdgfra$^{tm11(EGFP)Sor}$) (64). Mice were on a mixed background. Mice were genotyped with primers described in Supplemental Table S1. Angiopoietin-2 binding TIE2 activating human antibody (ABTAA) has been described previously (39, 40) and was a kind gift from Professor Gou Young Koh (Center for Vascular Research, Korea). Mice for treatment with ABTAA and for early gene regulation analysis were C57BL6/J mice from inhouse breeding, or WT mice from the above-mentioned breeding. Mice were injected with ABTAA (25 mg/kg body weight in PBS) intraperitoneally at indicated time points in Figure 1A and 6A. Control mice were injected with the same dose of human IgG Fc (AG714, Millipore) in PBS. Adult mice (8-16 weeks) were used for all experiments. Animals were housed on a 12h light-dark cycle with *ad libitum* access to water and standard chow. CKD was induced by UUO as previously described (5). UUO surgery was performed under anesthesia and animals received analgesia (Carprofen 5 mg/kg s.c., Norocarp, N-vet AB, Sweden) administered before surgery and daily two days post-surgery. Sham mice were subjected to all procedures except ligation of the ureter. Sham mice were used as baseline controls for left/right kidney perfusion in contrast-enhanced ultrasound imaging (Figure 1H). Both female and male mice were used in all experiments as the UUO model has previously not shown any

gender differences (92). The UUO model was chosen due to its reproducibility and inclusion of key features of human CKD, including peritubular capillary loss, tubulointerstitial fibrosis, and increased ANGPT2 expression. The contralateral kidney served as an internal control, allowing for reduction in animal numbers.

The total number of mice, gender distribution, and weight distribution can be found in Supplemental Table S2. All experiments used at least two independent litters, and a single animal was one experimental unit. The sample size and endpoints were selected based on our previous studies with the experimental model (5). No criteria for including or excluding animals were set and no data was excluded or defined as outliers. No randomization of treatment was used. Blinding was performed at different stages of the experiments. Animal care staff were unaware of treatment groups. Persons performing experimental measurements were blinded until grouped data analysis.

Renal perfusion measured with contrast imaging ultrasound

Renal perfusion was measured in isoflurane anesthetized mice on a heated platform utilizing a Vevo 2100 ultrasound system with a MS250 transducer and contrast imaging functionality software (Visual Sonics, Fujifilm). Mice were kept at a body temperature of 36-37°C, continuously measured with an anal probe. Mice were imaged from the back and the ultrasound transducer was fixed in place with a mechanical positioning system. Regular B-mode images were used to optimally position the mice to enable imaging of both kidneys at the same time. Mice were tail vein injected with 100 µl microbubble-based contrast agent (Vevo MicroMarker, VS-11913, Fujifilm Visual Sonics) from vials resuspended with 2 ml saline. Non-linear contrast images were acquired with General imaging in the Vascular package at 21 GHz. Images were analyzed for contrast intensity with Vevo Lab 3.2.6 (Fujifilm Visual Sonics) after manual marking region of

interest (ROI), cortex of both CL and UUO kidneys (Supplemental Figure S7). Perfusion was normalized to CL kidney for each mouse. Five sham operated WT mice were used in ultrasound graphs as comparison presented as the left kidney normalized to the right kidney.

Immunohistochemistry

Mice were euthanized with cervical dislocation; kidneys were dissected and renal capsules removed. Pieces of CL and UUO kidney were fixed for 4 hours at room temperature with 4% buffered formaldehyde (Histolab Products AB), washed with PBS followed by vibratome sectioning of 100 µm thick sections. After blocking and permeabilization (X0909, DAKO, with 0.25% Triton X100 for 2 hours), sections were incubated with primary antibodies overnight at 4ºC on a shaker. Antibodies are described in Supplemental Table S3. Appropriate secondary antibodies were added after washing with PBS containing 0.05% Tween-20 and incubated for 2 hours at room temperature. Nuclei were stained with Hoechst 33342 (Thermo Fisher Scientific).

RNA *in situ* hybridization

RNAscope® Multiplex Fluorescent Reagent Kit (v.2) (ACDBio) and TSA Plus reagents (Perkin Elmer) were used according to manufacturer's protocol for fresh frozen or fixed frozen sections with minor modifications. In brief, frozen tissue sections were cut at 14 µm thickness. Fresh frozen sections were first fixed with 4% buffered formaldehyde (Histolab Products AB) for 20 minutes at 4C, washed twice with 1xPBS and dehydrated through ethanol series. Fixed frozen sections were ready directly for dehydration. After dehydration, HRP was quenched with Bloxall blocking solution (Sp-6000, Vector Technologies) for 10 min at room temperature followed by Pretreat III solution for 30 min at room temperature. RNAscope®probes were hybridized on the sections for 2

h at 40°C after which fluorescence signals were developed and amplified according to manufacturer's protocol. Sections were mounted with ProLong®Gold mounting medium and images obtained using a confocal microscope (Leica Microsystems Sp8). RNAscope®probes used were (all from ACDBio): *Pecam1* (316721), *Pdgfb* (424651), *Angpt1* (449271), *Pdgfrb* (411381), *Pdgfra* (480661), and *Atp1a1* (569611).

Proliferation assay (EdU)

For EdU experiments, 0.25 mg EdU was injected i.p at indicated time points as shown in Supplemental Figure S5. Visualization of EdU+ cells was done with a Click-it plus EdU Imaging kit (C10640, Thermo Fisher) on 100 µm vibratome sections following the manufacturer's instructions.

Quantitative real-time PCR

RNAeasy Micro or Mini kit (Qiagen) was used to extract mRNA according to the manufacturer's protocol, followed by cDNA synthesis of 1 µg mRNA using iScript reverse transcription supermix (170-8841, BioRad). Real time PCR was performed using cDNA with Taqman Gene Expression master mix (4369016, Thermo Fisher Scientific) together with probes on a CFX-96 real time PCR system (BioRad). For primers, iTaq Universal SybrGreen supermix was used (172-5130, BioRad). Probes and primers are listed in Supplemental Table S4. Expression results were normalized to endogenous control *Hprt* or *Gapdh* and relative quantification was done using the Livak method ($2^{-\Delta\Delta CT}$) (93). FACS sorted cells were subjected to a preamplification step of 12 cycles with SsoAdvanced™ PreAmp Supermix (172-5160, Biorad) according to the manufacturer's instructions.

FACS of endothelial cells

Endothelial cells were isolated from CL and UUO kidneys of WT and *Tie2*^{iECKO} mice utilizing the *Cdh5*-TdTomato lineage labelling. At dissection, kidneys were cut into small pieces and digested into single cell suspension in MACS-C tubes with DMEM containing 0.13 U/ml Liberase TL (5401020001 Roche, Merck) and 1 ul/ml DNaseI (18068-15, Invitrogen) with rotation (200 rpm) in a gentleMACS dissociator (Miltenyi Biotec) for 20 minutes at 38°C. The suspension was passed through a 100 μm cell strainer and cells were washed two times by centrifugation at 300 x g for 5 min in DMEM containing 5 mM EDTA and 1% FBS. To reduce epithelial cell content from the cell suspension we utilized CD10-conjugated Dynabeads as previously described (47). Beads were prepared by adding 20 ul/ml rabbit monoclonal CD10 antibody to Protein G Dynabeads (10004D, Thermo Fisher Scientific) for 10 minutes at room temperature. After washing, CD10-Dynabeads were incubated with cell suspension for 10 minutes at room temperature, and cell solution remaining after magnet removal of CD10-Dynabead-bound cells was used for *Cdh5*-TdTomato isolation by BD FACS Melody. Cells were sorted directly into RLT lysis buffer (Qiagen) and RNA was purified as above.

Protein analysis

Snap frozen kidney tissues were homogenized in RIPA, buffer (89900, Pierce) containing protease and phosphatase inhibitors (4693116001, 4906845001, Merck). After centrifugation, supernatant was collected and measured for protein concentration using a BCA assay (Pierce), aliquoted and stored at -80°C. Protein lysates were used to measure protein concentrations by ELISA for TIE2 (MTE200, R&D Systems), ANGPT2 (MANG20, R&D Systems) and PDGFB (ab224879, Abcam)

according to the manufacturer's instructions.

For Western blotting, proteins were separated under reducing conditions on 4-12% Criterion XT Bis-Tris gels (3450123, Biorad), and then transferred using Criterion wet-transfer to 0.2 µm PVDF membranes (1620239, Biorad). Blots were blocked with EveryBlot blocking buffer (BioRad) and incubated overnight at 4°C with primary antibody (Supplemental Table S3). After washing and incubation with the appropriate HRP-conjugated secondary antibody, proteins were visualized using SuperSignal West Femto detection reagent (34096X4, Thermo Fisher Scientific). Membranes were cut to probe for different sized proteins. Band density was quantified with ImageJ (NIH).

For TIE2 immunoprecipitation, snap frozen kidney tissues were homogenized in ice-cold IP lysis buffer (Pierce 87787) with 2x protease and 1x phosphatase inhibitors as listed above and 1mM Na_3VO_4 and incubated 2h at 4°C in rotation. After centrifugation and BCA assay for protein concentration analysis, 2.5 mg of total kidney lysate or 1.5 mg lung lysate per sample was incubated with rabbit anti-TIE2 antibody (19157-1-AP, Thermo Fischer Scientific) overnight rotating at 4°C. The following day, lysates were incubated with Protein-A agarose beads (9863, Cell Signaling) for 2 h rotating at 4°C and subsequently washed four times with lysis buffer and denatured in 2x NuPage LDS sample buffer with denaturing agent (NP0007, Life Technologies) at 97°C for 5 min. Proteins were separated under reducing conditions on 4-12% Bis-tris gels (NuPage, Invitrogen) and transferred to 0.4 um PVDF membranes. Membranes were blocked with 3% BSA-TBST (0.1% Tween) and incubated two or three nights at 4°C with primary antibody (4G10, 05-321, Merck). After washing with TBS+0.1% Tween-20 and incubation with appropriate HRP conjugated secondary Ab (in BSA-TBST), membranes were developed with ECL™ Prime Western Blotting Detection Reagent (10308449, Cytiva Amersham™). The membranes were

stripped and reprobed with goat anti-mouse TIE2 Ab (AF762, R&D Systems). All antibodies are listed in Supplemental Table S3.

Blood samples for plasma ANGPT2 measurements were collected by heart puncture in isoflurane anesthetized mice and collected in tubes with K2 EDTA (Microvette 20.1339.100, Sarstedt). Samples were centrifuged at 2500 x g for 10 minutes, plasma collected and stored at -80ºC until analysis. ANGPT2 in plasma was measured by ELISA (MANG20, R&D Systems) in duplicates according to the manufacturer's instructions.

Transmission electron microscopy

For electron microscopy, kidneys were cut in 1 mm cubes, and immersion fixed in 2.5% glutaraldehyde (Ted Pella) and 1% paraformaldehyde (Merck) in 0.1 M phosphate buffer pH 7.4 and stored at 4°C until further processed. Samples were rinsed in 0.1 M phosphate buffer for 10 min followed by 1 h incubation in 1% osmium tetroxide (TAAB Laboratories Equipment) in 0.1 phosphate buffer. After rinsing in phosphate buffer, samples were dehydrated in alcohol followed by 5 min incubation in propylene oxide (TAAB Laboratories Equipment). Samples were then incubated for 1h in Epon Resin (TAAB Laboratories Equipment) and propylene oxide (1:1), followed by overnight incubation in 100% resin. Subsequently, samples were embedded in capsules with fresh resin for 1-2 h and then heat cured at 60°C for 48 h. The specimens were cut into semi thin sections, stained with Toluidine blue and examined in light microscopy. Ultrathin sections (60-70 nm) were cut in an EM UC7 Ultramicrotome (Leica) and placed on grids. Sections were contrasted with 5% uranyl acetate and Reynold's lead citrate and visualized in a Tecnai G2 Spirit BioTwin electron microscope (Thermo Fisher Scientific/FEI) at 80 kV with an Orius SC200 CCD camera and Gatan Digital Micrograph software (both from Gatan Inc.). Micrographs were

taken of peritubular capillaries and fenestrations were quantified as explained below.

Fluorescence microangiography

Fluorescence microangiography was used to visualize perfused vessels as described previously (94). In brief, 500 µl Fluospheres sulfate (0.02 µm, F8845, Thermo Fisher Scientific) was mixed with 4.5 ml low melting point agarose and kept at 41ºC. All solutions were preheated to 41ºC. Heart perfusion was carried out in dormicum/hypoderm sedated mice starting with 1 ml heparinized saline (100 IU/ml, H3149, Sigma), followed by 1 ml 3 M KCl, 5 ml PBS, and 5 ml Fluospheres/agarose mix. After perfusion, kidneys were dissected and put on ice for 20 min followed by fixation in 4% paraformaldehyde for 2 hours. Tissue was stored in PBS at 4ºC until further processing. For quantification, 100 µm vibratome sections were imaged in a Leica SP8 confocal microscope. The area of fluospheres perfusion was correlated to total vasculature (*Cdh5*-TdTomato) in each image.

Image quantification

For immunofluorescence analysis, kidney cortex was imaged (5 images/mouse, CL and UUO) at original magnification x400 using a Leica SP8 confocal microscope. Analysis was focused on cortex as medulla disappears at later timepoints after UUO. For estimation of fibrosis, aSMA and vimentin positive staining was quantified in each image using Otzu thresholding in ImageJ (NIH). Large arteries and glomeruli were excluded. Fibrotic area was expressed a percentage of the whole image area. Quantification of vascular area was done in the same way as above for endomucin and podocalyxin and correlated to the total number of nuclei per image. The number of nuclei was counted by utilizing Analyze Particles in ImageJ (NIH) with selection of positive areas of 50-800

pixels.

Proliferating endothelial cells (Ki67+ or EdU+) were counted in *Cdh5*-TdTomato+ nuclei in 5 image fields /mouse and correlated to the total number of endothelial nuclei per image (*Cdh5*-TdTomato+).

From EM micrographs, capillary fenestrations of peritubular and glomerular capillaries were semi-quantitatively graded and expressed as a score between 0-4, with 0: 0-5%, 1:6-25%, 2:26-50%, 3:51-75%, and 4:76-100% of the capillary length having fenestrations (i.e, a score of 4 in healthy kidneys), as previously described (16). To evaluate podocyte injury, the number of foot processes per glomerular basement membrane length was measured in Image J (NIH) and the foot process width was calculated as described previously (95).

An increased number of vacuoles was discovered during electron microscopy analysis and was therefore quantified on semithin sections stained with toluidine blue as the number of affected tubular segments correlated to the total number of tubular segments per image taken at an original magnification of x400. A tubular segment was defined as affected when vacuoles were present in the whole epithelial cell, from the luminal to the basolateral side (Figure 5A).

For densitometric analysis of TIE2 phosphorylation, Image Lab software (Bio-Rad) was used, and results expressed correlated to total TIE2 (pTIE2/total TIE2).

Human data

We utilized Nephroseq.org to obtain human data for *CDH5* (endothelial marker), *ANGPT2*, *PDGFB*, and *ANGPT1* from two different microarray datasets; renal biopsies with histopathological confirmed CKD (96), and renal biopsies from transplant patients with/without renal dysfunction (97). Data from living or cadaveric donors were combined. Data are presented

as Log2 expression and statistical differences comes from Nephroseq.

Bulk RNA-seq and data analysis

RNA was prepared from kidney tissue as above from all groups; IgG (n=8), ABTAA (n=7), *Veptp*^{WT} (n=7), *Veptp*^{KO} (n=8), *Pdgfb*^{WT} (n=4), and *Pdgfb*^{KO} (n=4). Two *Veptp*^{KO} CL and two *Pdgfb*^{WT} CL samples were lost in plate preparation. Kidneys from two sham operated *Pdgfb*^{WT} mice were used in the *Pdgfb*^{WT} CL group. Samples were run in quadruplets in a 384-well format. Library preparation and sequencing was performed as described previously (98). The uniquely indexed cDNA libraries from the 384-well plate were pooled and sequenced together on lane of a HiSeq3000 sequencer (Illumina). The 4 raw fastq sequences for each quadruple sample were merged and mapped with a standard STAR pipeline (version: 2.7.3a). The duplicated reads were filtered out using UMI-tools (version: 1.1.4). The gene expression counts summary was calculated using featureCounts function from the Subread package (version 1.4.6-p5) (99).

Differentially expressed genes (DEGs) were calculated by group comparisons utilizing R edgeR package (version: 3.40.2) (100) method. It applied an exact test between the groups (101) and the raw *P* values were corrected for multiple testing using the False Discovery Rate method (FDR). The FDR = 0.05 was set as threshold for significant differential expression. The raw counts data were normalized using the CPM method (Counts per Million). Gene expression heat maps are visualized using row Z-score calculated from CPM utilizing Heatmapper (102). Metascape v3.5.20240901 (70) were used for gene ontology (GO) enrichment of biological processes with DEGs from ABTAA and IgG treated groups. Statistical enrichment was calculated using the hypergeometric test with Benjamini-Hochberg correction to adjust for false discovery rates with a minimum overlap of 3 genes, a cut-off of $P<0.01$, and a minimum enrichment with 1.5. For

translatability, the analysis was done for the corresponding human gene annotation. The top 20 enrichment GO terms were visualized with heat maps based on -log10(*P*).

Statistical Analysis

GraphPad Prism 10 (GraphPad Software Inc.) was used for graphical representation and statistical analysis of data. Data are expressed as geometric mean±SD. Means between groups were compared using unpaired two-tailed Student's t-test (2 groups), or one-way ANOVA with Tukey's multiple comparisons post hoc test (≥3 groups). Many groups of data had an uneven distribution; hence data was natural log-transformed before statistical analysis as previously suggested (103). A *P* value less than 0.05 was considered significant. Please see "Bulk RNA-seq and data analysis" for details regarding analysis of bulk RNA-seq data.

Study approval

All procedures were approved in advance by the Uppsala Committee of Ethics of Animal Experiments (permit numbers C110/13, C100/15, 5.8.18-04862/2020, 5.8.18-04862/2023, and 5.8.18-20319/2024) and were conducted according to guidelines established by the Swedish Board of Agriculture. ARRIVE guidelines were used for reporting.

Data avaliability

RNA-seq data can be accessed from NCBI's Gene Expression Omnibus database, accession number GSE306281. All data used to support the findings of this study are included in the paper and the Supplementary Information is available from a searchable database at

https://heomics.shinyapps.io/Jeansson_lab_kidney_UUO/. Values for all data points in graphs are reported in the Supporting Data Values file (Supplemental File 5).

Author contributions

MJ concieved the study. RP, AM, LH, SN, and MJ participated in data acquisition, analysis, and interpretation. SEQ and CB provided key reagents and intellectual input. RP and MJ wrote the manuscript; all authors contributed to critical reading and editing.

Acknowledgements

The authors thank Jana Chmielniakova, Louise Larsson, Veronica Sundell, Pia Peterson, and Cecilia Olsson at Uppsala University for technical assistance. We are grateful to Gou Young Koh for providing ABTAA and Dietmar Vestweber for providing VEPTP antibody. We acknowledge the support from the BioVis platform at Uppsala University for assistance with FACS and electron microscopy and the Single Cell Core Facility Flemingsberg (SICOF) and Bioinformatics and Expression Analysis (BEA) for help with bulk RNA-seq. The use of Veptp floxed mice was made possible through core services and support from the Northwestern University George M. O'Brien Kidney Research Core Center (NU GoKidney), an NIH/NIDDK funded program (P30 DK114857).

This work was supported by the Knut and Alic Wallenberg Foundation Proof of Concept grant 2025 (MJ, CB), Novo Nordisk Foundation Pioneer Innovator grant NNF23OC0086927 (MJ), the European Foundation for the Study of Diabetes EFSD-BI-2023 (MJ), The Swedish Kidney Foundation F2021-0061 (MJ), F2022-0046 (MJ), F2023-0064 (MJ), The Knut and Alice Wallenberg Foundation 2024-0177 (MJ), 2015-0030 (CB), 2020-0057 (CB), The Swedish

Research Council 2012-865 (MJ), 2015-00550 (CB), Åke Wiberg Foundation 738866289 (MJ), Magnus Bergwall Foundation 2013-24942, 2014-00055 (MJ), IGP Young Investigator Award (MJ).

REFERENCES

1. Himmelfarb J, and Shankland SJ. Creating research infrastructure and functionality to address chronic kidney disease: the Kidney Research Institute. *Semin Nephrol.* 2009;29(5):457-66.
2. Collins AJ, et al. 'United States Renal Data System 2011 Annual Data Report: Atlas of chronic kidney disease & end-stage renal disease in the United States. *Am J Kidney Dis.* 2012;59(1 Suppl 1):A7, e1-420.
3. Global Burden of Metabolic Risk Factors for Chronic Diseases C. Cardiovascular disease, chronic kidney disease, and diabetes mortality burden of cardiometabolic risk factors from 1980 to 2010: a comparative risk assessment. *Lancet Diabetes Endocrinol.* 2014;2(8):634-47.
4. Foreman KJ, et al. Forecasting life expectancy, years of life lost, and all-cause and cause-specific mortality for 250 causes of death: reference and alternative scenarios for 2016-40 for 195 countries and territories. *Lancet.* 2018;392(10159):2052-90.
5. Loganathan K, et al. Angiopoietin-1 deficiency increases renal capillary rarefaction and tubulointerstitial fibrosis in mice. *PloS one.* 2018;13(1):e0189433.
6. Yuan HT, et al. Peritubular capillary loss after mouse acute nephrotoxicity correlates with down-regulation of vascular endothelial growth factor-A and hypoxia-inducible factor-1 alpha. *Am J Pathol.* 2003;163(6):2289-301.
7. Kairaitis LK, et al. HIF-1alpha expression follows microvascular loss in advanced murine adriamycin nephrosis. *Am J Physiol Renal Physiol.* 2005;288(1):F198-206.
8. Ohashi R, et al. Peritubular capillary regression during the progression of experimental obstructive nephropathy. *J Am Soc Nephrol.* 2002;13(7):1795-805.

9. Basile DP, et al. Renal ischemic injury results in permanent damage to peritubular capillaries and influences long-term function. *Am J Physiol Renal Physiol.* 2001;281(5):F887-99.
10. Matsumoto M, et al. Hypoperfusion of peritubular capillaries induces chronic hypoxia before progression of tubulointerstitial injury in a progressive model of rat glomerulonephritis. *J Am Soc Nephrol.* 2004;15(6):1574-81.
11. Namikoshi T, et al. Implication of peritubular capillary loss and altered expression of vascular endothelial growth factor in IgA nephropathy. *Nephron Physiol.* 2006;102(1):p9-16.
12. Ohashi R, et al. Peritubular capillary injury during the progression of experimental glomerulonephritis in rats. *J Am Soc Nephrol.* 2000;11(1):47-56.
13. Kang DH, et al. Role of the microvascular endothelium in progressive renal disease. *J Am Soc Nephrol.* 2002;13(3):806-16.
14. Ishii Y, et al. Injury and progressive loss of peritubular capillaries in the development of chronic allograft nephropathy. *Kidney Int.* 2005;67(1):321-32.
15. Choi YJ, et al. Peritubular capillary loss is associated with chronic tubulointerstitial injury in human kidney: altered expression of vascular endothelial growth factor. *Human pathology.* 2000;31(12):1491-7.
16. Babickova J, et al. Regardless of etiology, progressive renal disease causes ultrastructural and functional alterations of peritubular capillaries. *Kidney Int.* 2017;91(1):70-85.
17. Ehling J, et al. Quantitative Micro-Computed Tomography Imaging of Vascular Dysfunction in Progressive Kidney Diseases. *J Am Soc Nephrol.* 2016;27(2):520-32.

18. Kida Y, et al. Peritubular capillary rarefaction: a new therapeutic target in chronic kidney disease. *Pediatr Nephrol.* 2014;29(3):333-42.
19. Suri C, et al. Requisite role of angiopoietin-1, a ligand for the TIE2 receptor, during embryonic angiogenesis. *Cell.* 1996;87(7):1171-80.
20. Partanen J, and Dumont DJ. Functions of Tie1 and Tie2 receptor tyrosine kinases in vascular development. *Curr Top Microbiol Immunol.* 1999;237:159-72.
21. Augustin HG, et al. Control of vascular morphogenesis and homeostasis through the angiopoietin-Tie system. *Nat Rev Mol Cell Biol.* 2009;10(3):165-77.
22. Futrakul N, et al. Altered vascular homeostasis in chronic kidney disease. *Clinical hemorheology and microcirculation.* 2008;38(3):201-7.
23. Kim W, et al. COMP-angiopoietin-1 ameliorates renal fibrosis in a unilateral ureteral obstruction model. *J Am Soc Nephrol.* 2006;17(9):2474-83.
24. Jeansson M, et al. Angiopoietin-1 is essential in mouse vasculature during development and in response to injury. *J Clin Invest.* 2011;121(6):2278-89.
25. Lee S, et al. Renoprotective effect of COMP-angiopoietin-1 in db/db mice with type 2 diabetes. *Nephrol Dial Transplant.* 2007;22(2):396-408.
26. Dessapt-Baradez C, et al. Targeted glomerular angiopoietin-1 therapy for early diabetic kidney disease. *J Am Soc Nephrol.* 2014;25(1):33-42.
27. Chang FC, et al. Angiopoietin-2 inhibition attenuates kidney fibrosis by hindering chemokine C-C motif ligand 2 expression and apoptosis of endothelial cells. *Kidney Int.* 2022;102(4):780-97.

28. Lim HS, et al. Plasma vascular endothelial growth factor, angiopoietin-1, and angiopoietin-2 in diabetes: implications for cardiovascular risk and effects of multifactorial intervention. *Diabetes Care.* 2004;27(12):2918-24.
29. David S, et al. Angiopoietin 2 and cardiovascular disease in dialysis and kidney transplantation. *Am J Kidney Dis.* 2009;53(5):770-8.
30. Shroff RC, et al. Circulating angiopoietin-2 is a marker for early cardiovascular disease in children on chronic dialysis. *PloS one.* 2013;8(2):e56273.
31. David S, et al. Circulating angiopoietin-2 levels increase with progress of chronic kidney disease. *Nephrol Dial Transplant.* 2010;25(8):2571-6.
32. Winderlich M, et al. VE-PTP controls blood vessel development by balancing Tie-2 activity. *J Cell Biol.* 2009;185(4):657-71.
33. Drexler HCA, et al. Vascular Endothelial Receptor Tyrosine Phosphatase: Identification of Novel Substrates Related to Junctions and a Ternary Complex with EPHB4 and TIE2. *Molecular & cellular proteomics : MCP.* 2019;18(10):2058-77.
34. Carota IA, et al. Targeting VE-PTP phosphatase protects the kidney from diabetic injury. *The Journal of experimental medicine.* 2019;216(4):936-49.
35. Li Y, et al. Activation of Angiopoietin-Tie2 Signaling Protects the Kidney from Ischemic Injury by Modulation of Endothelial-specific Pathways. *J Am Soc Nephrol.* 2023.
36. Jung YJ, et al. Peritubular capillary preservation with COMP-angiopoietin-1 decreases ischemia-reperfusion-induced acute kidney injury. *Am J Physiol Renal Physiol.* 2009;297(4):F952-60.
37. Lee S, et al. Protective effect of COMP-angiopoietin-1 on cyclosporine-induced renal injury in mice. *Nephrol Dial Transplant.* 2008;23(9):2784-94.

38. Singh S, et al. Tubular Overexpression of Angiopoietin-1 Attenuates Renal Fibrosis. *PloS one.* 2016;11(7):e0158908.
39. Han S, et al. Amelioration of sepsis by TIE2 activation-induced vascular protection. *Sci Transl Med.* 2016;8(335):335ra55.
40. Park JS, et al. Normalization of Tumor Vessels by Tie2 Activation and Ang2 Inhibition Enhances Drug Delivery and Produces a Favorable Tumor Microenvironment. *Cancer cell.* 2016;30(6):953-67.
41. Kim J, et al. Tie2 activation promotes choriocapillary regeneration for alleviating neovascular age-related macular degeneration. *Sci Adv.* 2019;5(2):eaau6732.
42. Andrae J, et al. Role of platelet-derived growth factors in physiology and medicine. *Genes & Development.* 2008;22(10):1276-312.
43. Kida Y, and Duffield JS. Pivotal role of pericytes in kidney fibrosis. *Clin Exp Pharmacol Physiol.* 2011;38(7):467-73.
44. Chen YT, et al. Platelet-derived growth factor receptor signaling activates pericyte-myofibroblast transition in obstructive and post-ischemic kidney fibrosis. *Kidney Int.* 2011;80(11):1170-81.
45. Kramann R, et al. Perivascular Gli1+ progenitors are key contributors to injury-induced organ fibrosis. *Cell Stem Cell.* 2015;16(1):51-66.
46. Humphreys BD, et al. Fate tracing reveals the pericyte and not epithelial origin of myofibroblasts in kidney fibrosis. *Am J Pathol.* 2010;176(1):85-97.
47. Kuppe C, et al. Decoding myofibroblast origins in human kidney fibrosis. *Nature.* 2021;589(7841):281-6.

48. Vazquez-Liebanas E, et al. Adult-induced genetic ablation distinguishes PDGFB roles in blood-brain barrier maintenance and development. *Journal of Cerebral Blood Flow & Metabolism.* 2022;42(2):264-79.
49. Buhl EM, et al. Dysregulated mesenchymal PDGFR-beta drives kidney fibrosis. *EMBO molecular medicine.* 2020:e11021.
50. Lassila M, et al. Imatinib attenuates diabetic nephropathy in apolipoprotein E-knockout mice. *Journal of the American Society of Nephrology : JASN.* 2005;16(2):363-73.
51. Wang S, et al. Imatinib mesylate blocks a non-Smad TGF-beta pathway and reduces renal fibrogenesis in vivo. *FASEB J.* 2005;19(1):1-11.
52. Zoja C, et al. Imatinib ameliorates renal disease and survival in murine lupus autoimmune disease. *Kidney Int.* 2006;70(1):97-103.
53. Floege J, et al. A new look at platelet-derived growth factor in renal disease. *J Am Soc Nephrol.* 2008;19(1):12-23.
54. Floege J, et al. Novel approach to specific growth factor inhibition in vivo: antagonism of platelet-derived growth factor in glomerulonephritis by aptamers. *Am J Pathol.* 1999;154(1):169-79.
55. Ostendorf T, et al. Specific antagonism of PDGF prevents renal scarring in experimental glomerulonephritis. *J Am Soc Nephrol.* 2001;12(5):909-18.
56. Jia T, et al. The Role of Platelet-Derived Growth Factor in Focal Segmental Glomerulosclerosis. *J Am Soc Nephrol.* 2023;34(2):241-57.
57. Pohl L, and Schiessl IM. Endothelial cell plasticity in kidney fibrosis and disease. *Acta Physiol (Oxf).* 2023;239(2):e14038.

58. Chevalier RL, et al. Ureteral obstruction as a model of renal interstitial fibrosis and obstructive nephropathy. *Kidney Int.* 2009;75(11):1145-52.
59. Liu C, et al. Human endomucin is an endothelial marker. *Biochem Biophys Res Commun.* 2001;288(1):129-36.
60. Liang J, and Liu Y. Animal Models of Kidney Disease: Challenges and Perspectives. *Kidney360.* 2023;4(10):1479-93.
61. Zeisberg M, and Neilson EG. Biomarkers for epithelial-mesenchymal transitions. *J Clin Invest.* 2009;119(6):1429-37.
62. Mani SA, et al. The epithelial-mesenchymal transition generates cells with properties of stem cells. *Cell.* 2008;133(4):704-15.
63. Zeisberg EM, et al. Fibroblasts in kidney fibrosis emerge via endothelial-to-mesenchymal transition. *J Am Soc Nephrol.* 2008;19(12):2282-7.
64. Hamilton TG, et al. Evolutionary divergence of platelet-derived growth factor alpha receptor signaling mechanisms. *Molecular and cellular biology.* 2003;23(11):4013-25.
65. Chevalier RL. The proximal tubule is the primary target of injury and progression of kidney disease: role of the glomerulotubular junction. *Am J Physiol Renal Physiol.* 2016;311(1):F145-61.
66. Boor P, et al. PDGF and the progression of renal disease. *Nephrology Dialysis Transplantation.* 2014;29(suppl_1):i45-i54.
67. Uebelhoer M, et al. Venous malformation-causative TIE2 mutations mediate an AKT-dependent decrease in PDGFB. *Hum Mol Genet.* 2013;22(17):3438-48.
68. Si Y, et al. AKT/FOXO1 axis links cross-talking of endothelial cell and pericyte in TIE2-mutated venous malformations. *Cell Communication and Signaling.* 2020;18(1):139.

69. Ide S, et al. Ferroptotic stress promotes the accumulation of pro-inflammatory proximal tubular cells in maladaptive renal repair. *eLife.* 2021;10.
70. Zhou Y, et al. Metascape provides a biologist-oriented resource for the analysis of systems-level datasets. *Nature communications.* 2019;10(1):1523.
71. Bhatia D, et al. Mitochondrial dysfunction in kidney injury, inflammation, and disease: Potential therapeutic approaches. *Kidney research and clinical practice.* 2020;39(3):244-58.
72. Yuan HT, et al. Expression of angiopoietin-1, angiopoietin-2, and the Tie-2 receptor tyrosine kinase during mouse kidney maturation. *J Am Soc Nephrol.* 1999;10(8):1722-36.
73. Li H, et al. Comprehensive single-cell transcriptional profiling defines shared and unique epithelial injury responses during kidney fibrosis. *Cell Metab.* 2022;34(12):1977-98 e9.
74. Kirita Y, et al. Cell profiling of mouse acute kidney injury reveals conserved cellular responses to injury. *Proc Natl Acad Sci U S A.* 2020;117(27):15874-83.
75. Vikkula M, et al. Vascular dysmorphogenesis caused by an activating mutation in the receptor tyrosine kinase TIE2. *Cell.* 1996;87(7):1181-90.
76. Limaye N, et al. Somatic mutations in angiopoietin receptor gene TEK cause solitary and multiple sporadic venous malformations. *Nat Genet.* 2009;41(1):118-24.
77. Cho CH, et al. Long-term and sustained COMP-Ang1 induces long-lasting vascular enlargement and enhanced blood flow. *Circ Res.* 2005;97(1):86-94.
78. Hayashi M, et al. VE-PTP regulates VEGFR2 activity in stalk cells to establish endothelial cell polarity and lumen formation. *Nature communications.* 2013;4:1672.

79. Takahashi T, et al. Activation of STAT3/Smad1 is a key signaling pathway for progression to glomerulosclerosis in experimental glomerulonephritis. *J Biol Chem.* 2005;280(8):7100-6.
80. Basile DP, et al. Impaired endothelial proliferation and mesenchymal transition contribute to vascular rarefaction following acute kidney injury. *Am J Physiol Renal Physiol.* 2011;300(3):F721-33.
81. Liu Y. New Insights into Epithelial-Mesenchymal Transition in Kidney Fibrosis. *Journal of the American Society of Nephrology.* 2010;21(2):212-22.
82. Zhao HJ, et al. Endothelial nitric oxide synthase deficiency produces accelerated nephropathy in diabetic mice. *J Am Soc Nephrol.* 2006;17(10):2664-9.
83. Daly C, et al. Angiopoietin-1 modulates endothelial cell function and gene expression via the transcription factor FKHR (FOXO1). *Genes Dev.* 2004;18(9):1060-71.
84. Guo G, et al. Role of TNFR1 and TNFR2 receptors in tubulointerstitial fibrosis of obstructive nephropathy. *Am J Physiol.* 1999;277(5):F766-72.
85. Andrade-Oliveira V, et al. Inflammation in Renal Diseases: New and Old Players. 2019;10.
86. Thomson BR, et al. A lymphatic defect causes ocular hypertension and glaucoma in mice. *J Clin Invest.* 2014;124(10):4320-4.
87. Economides AN, et al. Conditionals by inversion provide a universal method for the generation of conditional alleles. *Proc Natl Acad Sci U S A.* 2013;110(34):E3179-88.
88. Pitulescu ME, et al. Inducible gene targeting in the neonatal vasculature and analysis of retinal angiogenesis in mice. *Nat Protoc.* 2010;5(9):1518-34.

89. Madisen L, et al. A robust and high-throughput Cre reporting and characterization system for the whole mouse brain. *Nat Neurosci.* 2010;13(1):133-40.
90. Enge M, et al. Endothelium-specific platelet-derived growth factor-B ablation mimics diabetic retinopathy. *EMBO J.* 2002;21(16):4307-16.
91. Hayashi S, and McMahon AP. Efficient recombination in diverse tissues by a tamoxifen-inducible form of Cre: a tool for temporally regulated gene activation/inactivation in the mouse. *Dev Biol.* 2002;244(2):305-18.
92. Yang HC, et al. Models of chronic kidney disease. *Drug discovery today Disease models.* 2010;7(1-2):13-9.
93. Livak KJ, and Schmittgen TD. Analysis of relative gene expression data using real-time quantitative PCR and the 2(-Delta Delta C(T)) Method. *Methods.* 2001;25(4):402-8.
94. Kramann R, et al. Fluorescence microangiography for quantitative assessment of peritubular capillary changes after AKI in mice. *J Am Soc Nephrol.* 2014;25(9):1924-31.
95. van den Berg JG, et al. Podocyte foot process effacement is not correlated with the level of proteinuria in human glomerulopathies. *Kidney Int.* 2004;66(5):1901-6.
96. Nakagawa S, et al. Molecular Markers of Tubulointerstitial Fibrosis and Tubular Cell Damage in Patients with Chronic Kidney Disease. *PloS one.* 2015;10(8):e0136994.
97. Flechner SM, et al. Kidney transplant rejection and tissue injury by gene profiling of biopsies and peripheral blood lymphocytes. *Am J Transplant.* 2004;4(9):1475-89.
98. Hagemann-Jensen M, et al. Single-cell RNA counting at allele and isoform resolution using Smart-seq3. *Nature biotechnology.* 2020;38(6):708-14.
99. Liao Y, et al. featureCounts: an efficient general purpose program for assigning sequence reads to genomic features. *Bioinformatics.* 2014;30(7):923-30.

100. Robinson MD, et al. edgeR: a Bioconductor package for differential expression analysis of digital gene expression data. *Bioinformatics.* 2010;26(1):139-40.
101. Robinson MD, and Smyth GK. Small-sample estimation of negative binomial dispersion, with applications to SAGE data. *Biostatistics.* 2008;9(2):321-32.
102. Babicki S, et al. Heatmapper: web-enabled heat mapping for all. *Nucleic Acids Res.* 2016;44(W1):W147-53.
103. Mamenko M, et al. Practical notes on popular statistical tests in renal physiology. *Am J Physiol Renal Physiol.* 2022;323(4):F389-F400.

FIGURES

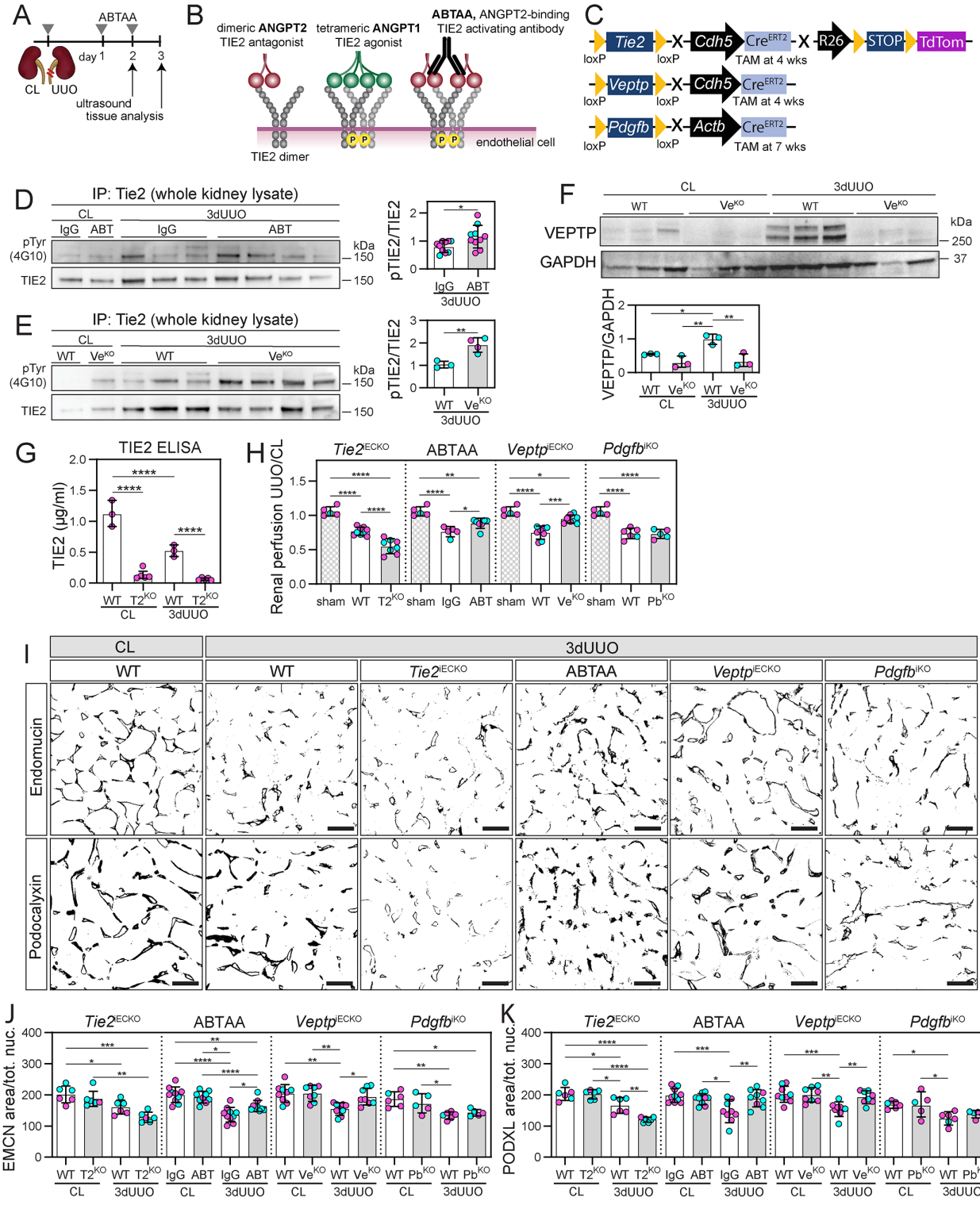

Figure 1. Pharmacological or genetic activation of TIE2 improves renal perfusion and prevents capillary rarefaction following experimental CKD. (**A**) Schematic diagram of the experimental set-up with unilateral ureterer obstruction (UUO), contralateral control kidney (CL),

and ABTAA (or IgG) administration. (**B**) Schematic diagram of ABTAA function, and (**C**) inducible conditional mouse lines used in the study. (**D** and **E**) pTIE2/TIE2 in 3-day UUO kidneys in ABTAA (ABT) and *Veptp*^{iECKO} (Ve^{KO}) mice, respectively. Data is based on n=3-10 mice/group and 3 (**D**) and 1 (**F** and **E**) blots, see Supplemental Figure S2. (**F**) VEPTP in kidney lysates from CL and 3-day UUO kidneys in WT and *Veptp*^{iECKO} (Ve^{KO}) mice. Data is based on n=3/group and 1 blot, see Supplemental Figure S2. (**G**) TIE2 protein measured by ELISA in kidney homogenates from CL and 3-day UUO kidneys in *Tie2*^{iECKO} (T2^{KO}) mice. Data is based on n=3-5 mice/group. (**H**) Renal perfusion measured with ultrasound contrast imaging in 2-day UUO/CL kidneys from ABTAA treated (ABT), *Veptp*^{iECKO} (Ve^{KO}), *Tie2*^{iECKO} (T2^{KO}), and *Pdgfb*^{iKO} (Pb^{KO}) mice and their respective controls. The same group of sham-operated mice was used to establish baseline perfusion levels for comparison to UUO-injured kidneys. Data is based on n=5-8 mice/group. (**I-K)** Immunohistochemistry and quantification from renal cortex for endothelial markers (endomucin and podocalyxin) in 3-day UUO kidneys for ABTAA treated, *Veptp*^{iECKO}, *Tie2*^{iECKO}, and *Pdgfb*^{iKO} mice and their controls. Data is based on n=5-11 mice/group and >600 images/marker. Scale bars, 50 μm. Data represent mean ± SD and each symbol represents 1 mouse (females: magenta, males: cyan). **P*<0.05, ***P*<0.01, ****P*<0.001, *****P*<0.0001 with 1-way ANOVA and Tukey's post hoc test (**F**, **G**, **H**, **J**, and **K**) or unpaired 2-tailed Student's *t* test (**D** and **E**).

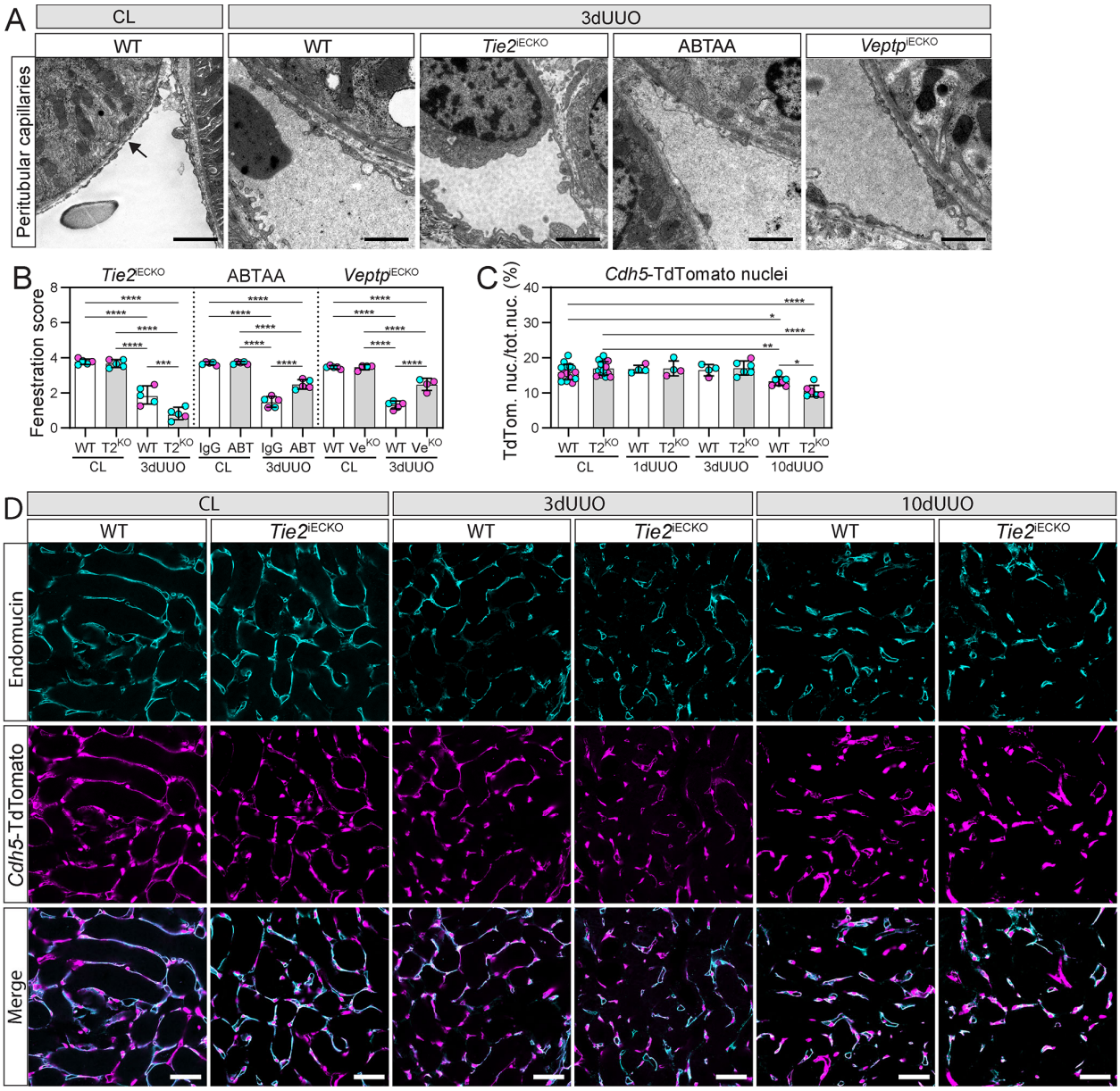

Figure 2. Pharmacological or genetic TIE2 activation prevents UUO-induced endothelial injury. (**A, B**) Semiquantitative grading of capillary length with fenestrations from micrographs of peritubular capillaries in 3-day UUO kidneys from ABTAA treated (ABT), *Veptp*^{iECKO} (Ve^{KO}), and *Tie2*^{iECKO} (T2^{KO}) mice. Data is based on n=4-5 mice/group and scoring of 892 micrographs. Scoring based on percent of endothelium with fenestrations; 0: 0-5%, 1: 6-25%, 2: 26-50%, 3: 51-75%, and 4: 76-100%. The fenestrated endothelium is indicated by an arrow. Scale bars, 2 µm. (**C**) Quantification of endothelial nuclei in *Tie2*^{iECKO} and WT mice from 1-, 3-, and 10-day UUO kidneys. Data is based on n=4-7 mice/group and 310 images were quantified. (**D**) Representative image with immunohistochemistry for endomucin (cyan) together with the endothelial *Cdh5*-Tdtomato lineage tracer (magenta). Scale bars, 50 µm. Data represent mean±SD and each symbol represents 1 mouse (females: magenta, males: cyan). **P*<0.05, ***P*<0.01, ****P*<0.001, *****P*<0.0001 with 1-way ANOVA and Tukey's post hoc test (**B** and **C**).

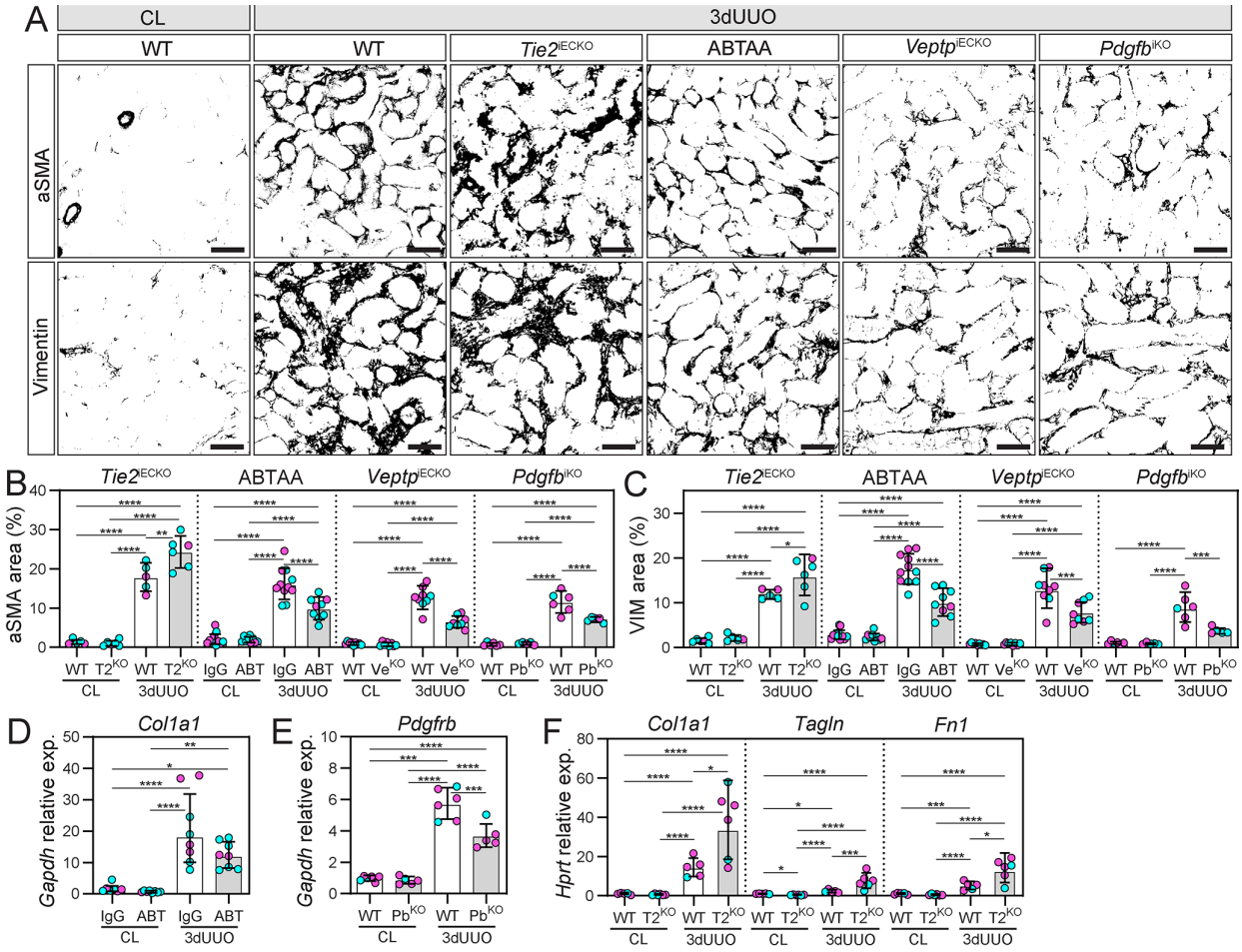

Figure 3. Pharmacological or genetic TIE2 activation prevents UUO-induced tubulointerstitial fibrosis. (**A-C**) Immunohistochemistry and quantifications from renal cortex for fibrosis markers (aSMA and vimentin) in 3-day UUO kidneys from ABTAA treated (ABT), *Veptp*^{iECKO} (Ve^{KO}), *Tie2*^{iECKO} (T2^{KO}), and *Pdgfb*^{iKO} (Pb^{KO}) mice and their controls. Data is based on n=5-11 mice/group and quantifications from >600 images/marker. Scale bars, 50 µm. (**D**) Renal *Col1a1* expression in ABTAA treated mice. Data is based on n=6 mice/group. (**E**) Renal *Pdgfrb* expression in *Pdgfb*^{iKO} mice. Data is based on n=5-6 mice/group. (**F**) Gene expression of *Col1a1*, *Tagln*, and *Fn1* in 3-day UUO kidneys from *Tie2*^{iECKO} mice. Data is based in n=5-6 mice/group. Data represent mean±SD and each symbol represents 1 mouse (females: magenta, males: cyan). **P*<0.05, ***P*<0.01, ****P*<0.001, *****P*<0.0001 with 1-way ANOVA and Tukey's post hoc test (**B-F**).

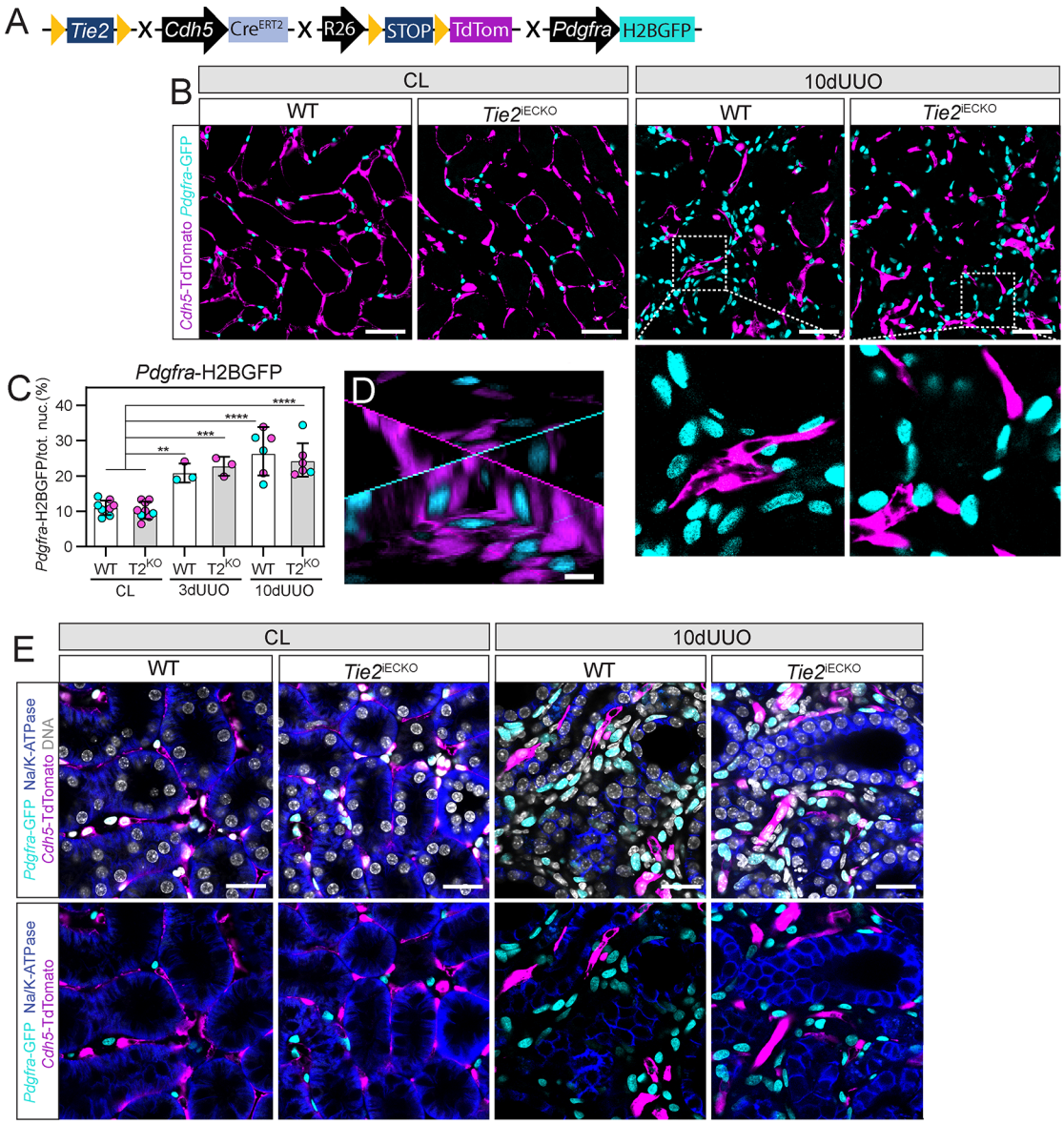

Figure 4. UUO-induced tubulointerstitial fibrosis is not the result of EndoMT. (**A**) Breeding strategy for *Tie2*^{iECKO} mice with endothelial lineage tracer and myofibroblast reporter. (**B, C**) Imaging and quantification of *Pdgfra*-H2BGFP positive nuclei (cyan) in renal cortex of 3- and 10-day UUO kidneys in WT and *Tie2*^{iECKO} (T2^{KO}) mice. Data is based on n=3-6 mice/group and quantifications from >180 images. Scale bars, 50 µm. (**D**) Representative confocal image stack (30 µm) from renal cortex showing *Cdh5*-TdTomato (magenta) and *Pdgfra*-H2BGFP (cyan) in renal cortex 10 days after UUO in a *Tie2*^{iECKO} mouse. Scale bar, 10 µm. (**E**) Confocal images from renal cortex showing tubular epithelial marker NaK/ATPase (blue), *Pdgfra*-GFP (cyan) and *Cdh5*-TdTomato (magenta) 10 days after UUO in WT and Tie2^{iECKO} mice. Representative image of *n* = 3 mice per group. Scale bars, 25 µm. Data in graphs represent mean±SD and each symbol represents 1 mouse (females: magenta, males: cyan). ***P*<0.01, ****P*<0.001, *****P*<0.0001 with 1-way ANOVA and Tukey's post hoc test (**C**).

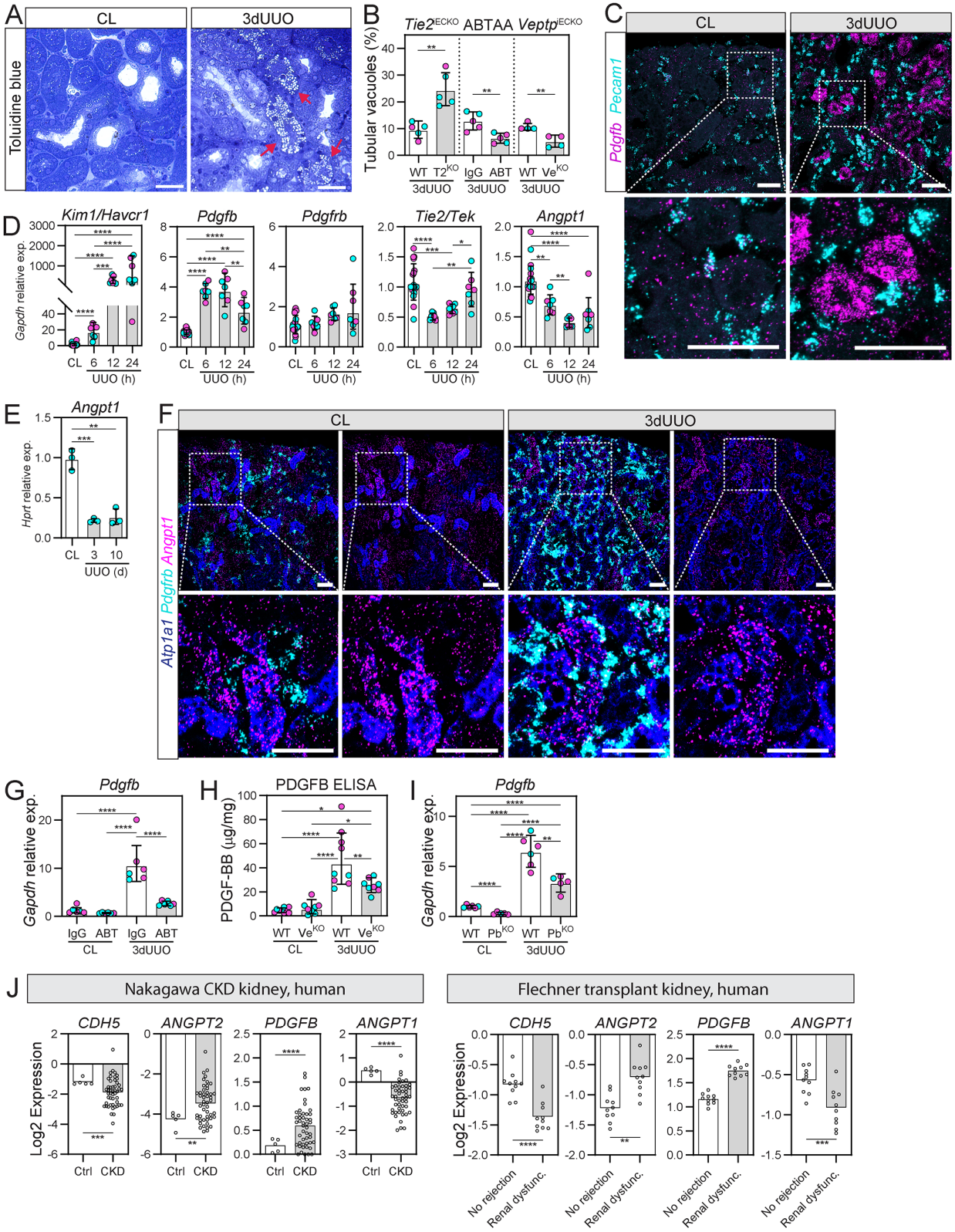

Figure 5. Pharmacological or genetic TIE2 activation prevents UUO-induced tubular injury and PDGFB expression. (**A**) Tubular segments with pathological vacuoles (red arrow) in kidney sections stained with Toluidine blue. (**B**) Quantification of tubular segments with vacuoles for

ABTAA treated (ABT), *Veptp*^{iECKO} (Ve^{KO}), and *Tie2*^{iECKO} (T2^{KO}) mice. Data is based on n=4-5 mice/group and >10,000 tubular cross sections. (**C**) RNA-ISH for *Pecam1* (cyan) and *Pdgfb* (magenta) in 3-day UUO kidney. Representative image of n=4 mice. Scale bars, 50 µm. (**D, E**) Gene expression of *Kim1*, *Pdgfb*, *Pdgfrb*, *Tie2*, and *Angpt1* in UUO kidneys from indicated timepoints. Data is based on n=3-7 mice/group. (**F**) RNA-ISH for *Angpt1* (magenta), mesenchymal marker *Pdgfrb* (cyan), and tubular marker *Atp1a1* (blue) in 3-day UUO kidneys. Representative image of n=3 mice Scale bars, 50 µm. (**G-I**) Expression of Pdgfb/PDGFB in 3-day UUO kidneys from ABTAA treated (ABT), *Veptp*^{iECKO} (VeKO), and *Pdgfb*^{iKO} (Pb^{KO}) mice. Data based on n=5-9 mice/group. (**J**) Patient data retrieved from NephroSeq for renal *CDH5* (endothelial marker), *ANGPT2*, *PDGFB*, and *ANGPT1* expression in CKD and renal dysfunction compared to normal man kidney. Data in graphs (**B**, **D**, **E**, **G**, **H**, **I**) represent mean±SD and each symbol represents 1 mouse (females: magenta, males: cyan). $^{**}P<0.01$, $^{***}P<0.001$, $^{****}P<0.0001$ with 1-way ANOVA. Human data (**J**) represents Log2 expression and statistical differences from NephroSeq, see Methods.

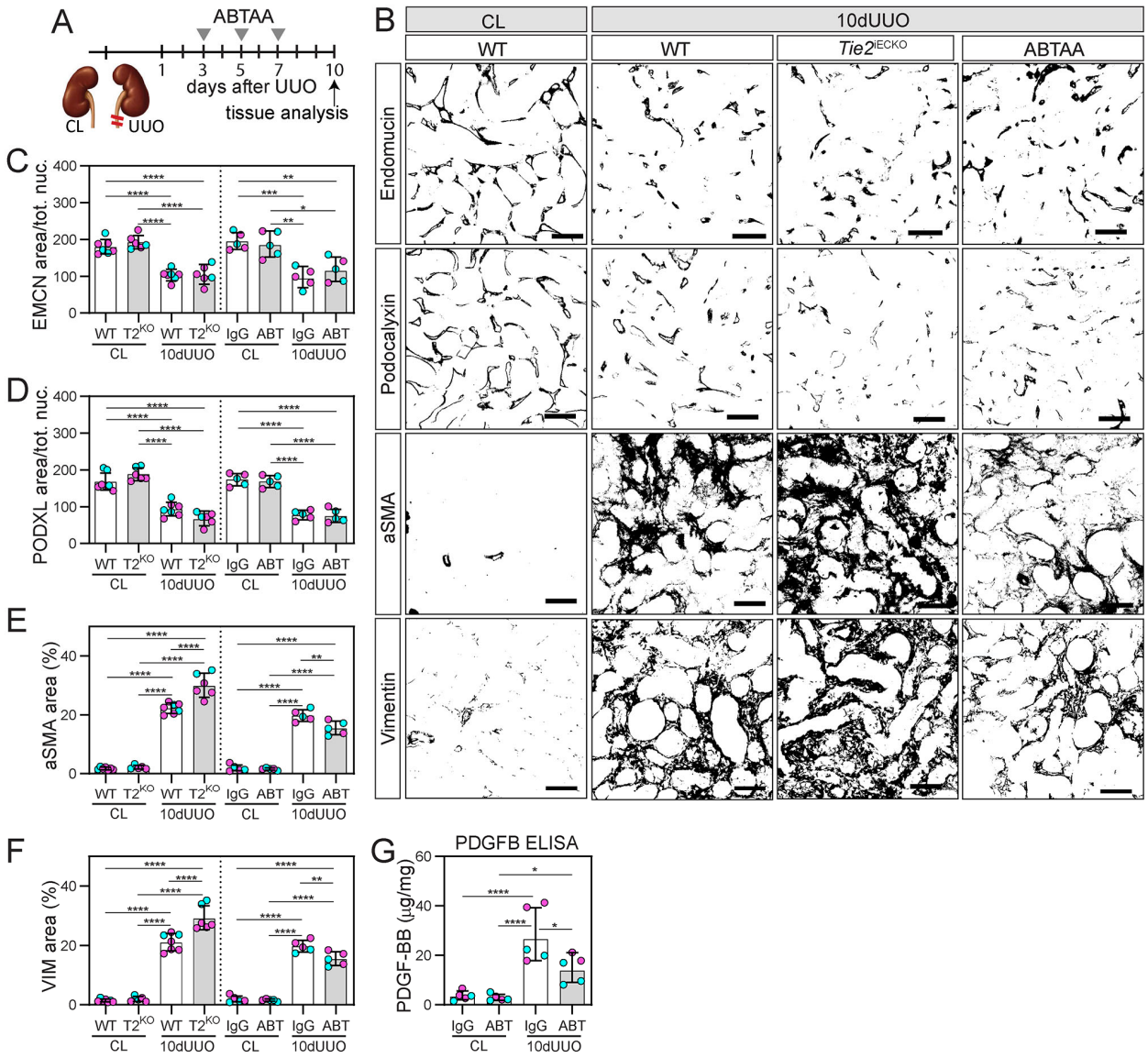

Figure 6. Post-injury treatment with ABTAA slows progression of fibrosis. (**A**) Schematic diagram of administration of ABTAA for evaluation in 10-day UUO kidneys. (**B-F**) Immunohistochemistry of renal cortex for capillary density (endomucin, podocalyxin) and tubulointerstitial fibrosis (aSMA, vimentin) in 10-day UUO kidneys from ABTAA treated mice (ABT) and *Tie2*^{iECKO} ($T2^{KO}$) mice. Data is based on n=6-7 mice/group and quantification of >220 images/marker. Scale bars, 50 µm. (**E**) Protein concentration for PDGFB in 10-day UUO kidneys from ABTAA treated (ABT) mice. Data is based on n=5 mice/group. Data in graphs represent mean±SD and each symbol represents 1 mouse (females: magenta, males: cyan). **P*<0.05, ***P*<0.01, ****P*<0.001, *****P*<0.0001 with 1-way ANOVA and Tukey's post hoc test.

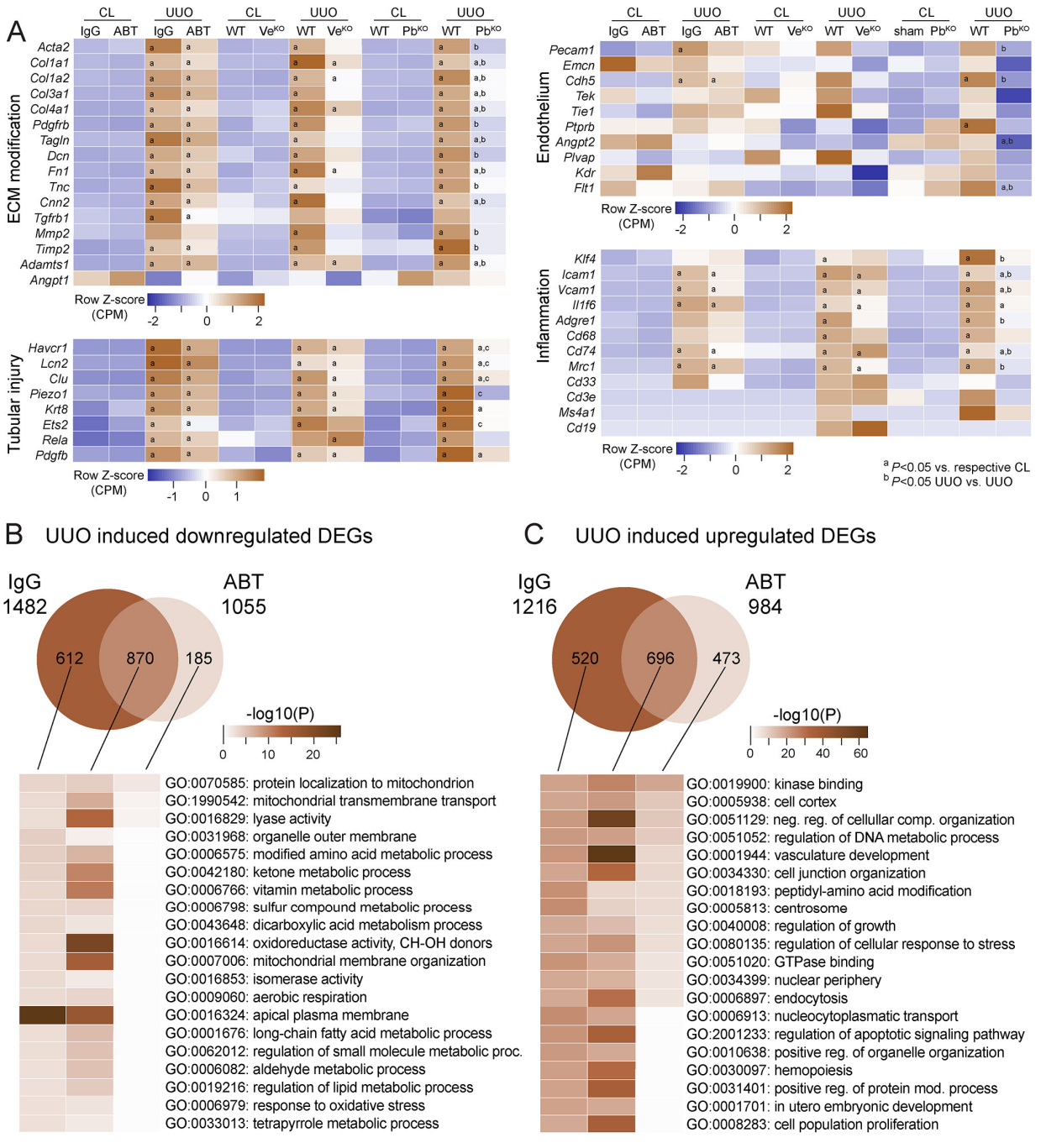

Figure 7. Pharmacological or genetic TIE2 activation, or inhibition of PDGFB signaling, protect the kidney transcriptome following UUO injury. Bulk RNA-seq of 3-day UUO kidneys. (**A**) Heatmaps of genes relevant for ECM modifications, tubular injury, endothelium, and inflammation in ABTAA/IgG-treated (n=7-8), *Veptp*^{iECKO}/*Veptp*^{WT} (n=6-8), and *Pdgfb*^{iKO}/*Pdgfb*^{WT} (n=4) mice. [a]*P*<0.05 vs. respective CL, [b] [c]*P*<0.05 UUO vs. UUO. (**B**, **C**) Venn diagrams of downregulated and upregulated DEGs and Metascape analysis of linked gene ontology (GO) for DEGs.

Supplementary materials

Supplemental Methods and Results

Supplemental File 1: Bulk RNA-seq, CPM and raw counts

Supplemental File 2: Bulk RNA-seq, statistical comparisons

Supplemental File 3: Bulk RNA-seq, DEGs

Supplemental File 4: Bulk RNA-seq, Metascape analysis of DEGs

Supplemental File 5. Supporting Data Values file